Comparison of Two Planning Methods for Heterogeneity Correction in Planning Total Body Irradiation

Emily Elizabeth Flower

BAppSci (Medical Biophysics and Instrumentation)

School of Applied Sciences

RMIT University

December 2005

Statement

Except where due acknowledgement or reference has been made, the work in this thesis is original. To the best of my knowledge no other person's work has been used without due acknowledgement. This work has not been previously submitted in whole or part to qualify for any other degree. The experimentation and analysis of data are largely my own work, with the support and constructive assistance of my supervisors. This thesis is the result of work completed after the official commencement of this degree.

Emily Flower

December 2005

Acknowledgements

I would firstly like to acknowledge my supervisors, Prof Peter Johnston and Mr Romuald Gajewski. Their support and direction have been beneficial in this project.

My fellow Medical Physicists from Westmead Hospital, particularly the Director of Medical Physics, Mr Gary Arthur, for allowing time and resources to work on this project and for helping with more constructive criticism. Also Miss Alison Gray who proofread my thesis.

Mr Dennis Payne, from the Biomedical Engineering Department at Westmead Hospital, for obtaining and machining the Perspex^{TM} and cork inserts required for my phantom.

I also acknowledge the working program for TLD dosimetry and TBI treatments that already exists at Westmead Hospital, including the design of the current 2D planning protocol, treatment protocol and TBI cradle design.

I thank my family and friends for their unfailing support and encouragement throughout my studies and particularly during the preparation of this thesis.

Finally, as a spirit filled Christian I acknowledge the work of God in my life. As a child I was diagnosed as having learning difficulties and my parents were told not to expect me to finish school. I started school with an integration aid, and my early reports followed the predicted pattern. However, my God healed me, to the extent that I have prepared this thesis for my Masters Degree. Having the Holy Spirit in my life also is a great source of strength and comfort in my life. I thank God for my life and the opportunity to complete this degree.

Summary

Total body irradiation (TBI) is often used as part of the conditioning process prior to bone marrow transplants for diseases such as leukemia. By delivering radiation to the entire body, together with chemotherapy, tumour cells are killed and the patient is also immunosupressed. This reduces the risk of disease relapse and increases the chances of a successful implant respectively.

TBI requires a large flat field of radiation to cover the entire body with a uniform dose. However, dose uniformity is a major challenge in TBI. (AAPM Report 17) The ICRU report 50 recommends that the dose range within the target volume remain in the range of –5% to +7%. Whilst it is generally accepted that this is not possible for TBI, it is normally clinically acceptable that ±10% of the prescribed dose to the whole body is sufficiently uniform, unless critical structures are being shielded.

TBI involves complex dosimetry due to the large source to treatment axis distance (SAD), dose uniformity and flatness over the large field, bolus requirements, extra scatter from the bunker walls and floor and large field overshoot. There is also a lack of specialised treatment planning systems for TBI planning at extended SAD.

TBI doses at Westmead Hospital are prescribed to midline. Corrections are made for variations in body contour and tissue density heterogeneity in the lungs using bolus material to increase dose uniformity along midline.

Computed tomography (CT) data is imported into a treatment planning system. The CT gives information regarding tissue heterogeneity and patient contour. The treatment planning system uses this information to determine the dose distribution. Using the dose ratio between plans with and without heterogeneity correction the effective chest width can be calculated. The effective chest width is then used for calculating the treatment monitor units and bolus requirements.

In this project the tissue heterogeneity corrections from two different treatment planning systems are compared for calculating the effective chest width. The treatment planning systems used were Pinnacle^{TM}, a 3D system that uses a convolution method to correct for tissue heterogeneity and calculate dose. The other

system, Radplan™, is a 2D algorithm that corrects for tissue heterogeneity using a modified Batho method and calculates dose using the Bentley – Milan Algorithm. Other possible differences between the treatment planning systems are also discussed.

An anthropomorphic phantom was modified during this project. The chest slices were replaced with Perspex™ slices that had different sized cork and Perspex™ inserts to simulate different lung sizes. This allowed the effects of different lung size on the heterogeneity correction to be analysed. The phantom was CT scanned and the information used for the treatment plans.

For each treatment planning system and each phantom plans were made with and without heterogeneity corrections. For each phantom the ratio between the plans from each system was used to calculate the effective chest width. The effective chest width was then used to calculate the number of monitor units to be delivered.

The calculated dose per monitor unit at the extended TBI distance for the effective chest width from each planning system is then verified using thermoluminescent dosimeters (TLDs) in the unmodified phantom. The original phantom was used for the verification measurements as it had special slots for TLDs.

The isodose distributions produced by each planning system are then verified using measurements from Kodak EDR2 radiographic film in the anthropomorphic phantom at isocentre. Further film measurements are made at the extended TBI treatment SAD.

It was found that only the width of the lungs made any significant difference to the heterogeneity correction for each treatment planning system. The height and depth of the lungs will affect the dose at the calculation point from changes to the scattered radiation within the volume. However, since the dose from scattered radiation is only a fraction of that from the primary beam, the change in dose was not found to be significant.

This is because the calculation point was positioned in the middle of the lungs, so the height and depth of the lungs didn’t affect the dose at the calculation point.

The dose per monitor unit calculated using the heterogeneity correction for each treatment planning system varied less than the accuracy of the TLD measurements. The isodose distributions measured by film showed reasonable agreement with those calculated by both treatment planning systems at isocentre and a more uniform distribution at the extended TBI treatment distance.

The verification measurements showed that either treatment planning system could be used to calculate the heterogeneity correction and hence effective chest width for TBI treatment planning.

TABLE OF CONTENTS

LIST OF DIAGRAMS

LIST OF TABLES

Chapter One – Introduction

Radiation Oncology is a branch of medicine dedicated to the use of ionising radiation to destroy cancer cells. For most cases, the cancer is a solid tumour and the radiation dose is delivered to the tumour and any likely sites of spread such as lymph nodes, as a localised treatment. Systemic treatments such as chemotherapy are also available. For systemic diseases such as leukaemia, localised treatment is not an option, as the entire body requires treatment.

Part of the treatment available for diseases such as leukaemia is a bone marrow transplant (BMT). Total body irradiation (TBI) is a part of the treatment given prior to a bone marrow transplant. TBI involves the use of megavoltage photon beams to deliver radiation to the entire body. Historically gamma ray beams from a Cobalt – 60 source were used but now linear accelerators are used for TBI throughout Australia. The radiation destroys the tumour cells and suppresses the immune system, reducing the risk of disease relapse and increasing the chance that the transplant will be successful.

BMT success rates are such that “patients with acute myeloid leukemia transplanted in first remission can now expect an approximately 50 to 60% likelihood of long-term disease-free survival. Similar probabilities are also achievable after transplantation of adults with acute lymphoblastic leukemia in first remissions. Probability of relapse correlates with remission status at the time of the transplant, ranging from 20% in first remission to 60% with more advanced disease. Long-term survival for patients with chronic myelocytic leukemia who receive BMT in the phase of remission is 60 to 70%”. (Merck Manual 2005)

As with all radiation therapy the treatment process begins with collection of general linear accelerator data during commissioning, which is used for treatment planning. Then the patient data required for dose calculation is collected. This can involve physical measurements of patient size and contour, radiographic imaging and/or computed tomography (CT) scanning. How the patient will be positioned during treatment is also determined at this time, as well as the position of any accessories used during treatment, such as the beam spoiler. This process is known as patient simulation.

The next stage for all radiation therapy treatments is known as treatment planning. During planning the beam arrangement and fluence is determined and the number of monitor units to be delivered so the prescribed dose to be given is calculated. Evaluation tools such as isodose map and dose volume histograms can be used to verify the target is receiving the correct dose and that organs at risk are receiving an acceptable dose, i.e. the dose to critical structures is as low as possible.

Different methods can be used to calculate dose for radiation treatment. This thesis investigates whether there are any differences between two planning methods for TBI at extended distances. The two methods are a 2D planning Bentley – Milan algorithm with modified Batho heterogeneity correction method and 3D planning convolution method. This included testing any differences due to different lung sizes. The results were verified with thermoluminescent dosimeters (TLD) and film measurements in an anthropomorphic phantom.

Anthropomorphic phantoms can be used to verify the dose distribution and absolute doses at points predicted by treatment planning systems. These measurements are made using ionising radiation detectors such as radiographic film and TLDs. This verification process evaluates the different methods of calculating dose for radiation treatment.

Only after the accuracy of a dose calculation method has been verified with such measured data can this method be used to calculate the number of monitor units for each beam of a patient treatment.

During treatment the patient is setup the same way as they were positioned during the patient simulation process and the treatment is delivered as planned. Invivo dosimetry, where measurements are made with detectors on or inside the patient during treatment, is another verification method. Invivo dosimetry can be used to determine the accuracy of the entire treatment chain from simulation to treatment as described above.

In chapter two a literature review is completed, to give a background to this research project. This begins by covering the clinical aspects of TBI, including the short term and long term side effects of TBI.

Some of the methods used for delivering TBI are discussed in chapter two, including the requirements of the delivery systems. The various methods for tissue compensation such as bolus material or metal compensators are also discussed. These can either compensate for variations in patient shape or for low density regions, to ensure the same effective pathlength to the patient's midline.

For radiation therapy treatment planning to occur, parameters about the treatment beam, such as its profile and percentage depth dose curve, as well various factors related to beam scatter need to be determined. The beam data required for TBI treatment planning is discussed.

Methods for planning TBI treatment are discussed, including tissue density heterogeneity corrections. The algorithms used by both treatment planning systems for calculating radiation dose are also described. Factors that influence the overall dose distribution and more specifically lung dosimetry during TBI are also discussed. The lung is of particular interest because lung tissue has a lower density than muscle tissue so offers less attenuation to radiation, affecting the dosimetry. Lung tissue is also radiation sensitive as demonstrated by one of most serious morbidities from TBI, radiation pneumonitis.

Methods for verifying the calculated dose are also described. Some of the characteristics of TLDs and films, two of the most commonly used dosimeters for verification measurements, are also discussed.

In chapter three the project methodology is discussed. A phantom was designed by modifying an anthropomorphic phantom with a specially developed chest insert to replace the original phantom chest slices. This enabled different lung sizes to be simulated. This phantom was then scanned with its different lung sizes.

The CT datasets were then used to create plans for the various different lung sizes. Radplan^{TM} calculates dose using the Bentley – Milan algorithm and corrects for

heterogeneities using a modified Batho technique. Pinnacle^{TM} (ADAC laboratories, Milpitas, CA) uses a convolution method to calculate dose distributions.

For each treatment planning system the plans were repeated without tissue heterogeneity corrections. The ratio between the plan with heterogeneity correction and without for each system was then used to calculate the effective chest width. The effective chest width was then used to calculate the number of monitor unitFs.

To verify the planning processes worked as expected, plans were made using the unmodified RANDO^{TM} phantom with TLD slots. The planned point doses were verified by placing TLDs within the phantom and delivering a treatment at the extended TBI SAD of 400 cm to the phantom as planned. Comparisons were made between the measured dose and the planned dose.

Kodak EDR2 radiographic film was also placed into the phantom to measure the delivered dose distribution. This measured dose distribution was then compared to the planned dose distributions from each planning system. This process was repeated at 100 cm SAD (isocentre) and the extended TBI treatment distance of 400 cm.

Chapter four presents the results calculated using data from the treatment planning systems. The effective chest width is calculated using the ratio between the monitor units from the treatment planning systems with and without heterogeneity correction. The dose per monitor unit verification measurements with TLDs and dose distribution verification measurements with radiographic film are also presented.

Chapter five discusses the results of the planning studies and the phantom verification measurements. It also discusses the errors and uncertainties pertaining to this study and clinical TBI treatments. Suggestions are made for future work.

Chapter six offers the conclusions of the study. Whilst a difference was calculated, this difference was smaller than the accuracy of the TLD measurements. Hence no significant difference could be detected between the two planning methods. The film measurements showed reasonable agreement with both planning systems at 100 cm

SAD and significant differences at 400 cm SAD. Either method could be used clinically.

Chapter Two – Literature Review

Clinical Aspects

TBI with megavoltage photon beams is a radiotherapeutic procedure that is used for the treatment of haematological disorders and disseminated malignancies such as acute leukaemia, lymphomas or aplastic anaemia. It is part of the cytoreductive conditioning program prior to a bone marrow or stem cell transplants, along with chemotherapy. (AAPM report 17; Harden, 2001)

TBI helps remove tumour cells from the body and also results in adequate immunosuppression for a successful graft. (Galvin, 1980; Kim, 1980) This is due to the ablation of normal hemopoietic and lymphoid cells, which helps facilitate engraftment of the new cells. With TBI treatments there are no sanctuary sites (due to radiation penetration throughout entire body) or evolution of clonal resistance. It is also likely that chemoresistant leukemic cells will remain radiosensitive (Doughty, 1987).

As with all treatment modalities, it is desirable to have the maximum possible therapeutic ratio, ie, high disease control with minimal normal tissue toxicity, especially to critical tissues. (Obcemea, 1992)

Short-term side effects of TBI include mucositis, alopecia, dysphagia, diarrhoea, parotitis, erythema, pneumonitis, veno-occlusive disease and all the attendant risks of prolonged pancytopaenia. The long-term risks include ophthalmological sequelae (cataracts), endocrinological sequelae (reduced pituitary function), neurological sequelae, infertility and increased risk of secondary malignancies. (Harden, 2001; Quast, 1987) Following the BMT there is also a risk of graft versus host disease. (Yuille, 1983) The dose tolerance of various different normal tissues for non-stochastic radiation effects is discussed in the ICRP report 44.

TBI was originally given as a single fraction (Harden, 2001) but side effects can be reduced with fractionated treatments, based on radiobiology principles of preferential

normal tissue repair. Studies have found that fractionated TBI can reduce side effects whilst still producing good anti-leukemic outcomes. (Cosset, 1994; Shank, 1983)

Dose uniformity is a major challenge in TBI. (AAPM Report 17) Under-dosages will increase the risk of relapse whilst overdose, especially to critical organs (lungs, eye lens etc), will increase toxicity. According to the ICRU report 50 the dose range within the target volume should remain in the range of –5% to +7%. So for TBI the ideal situation is that the whole body including the skin receives a dose within –5% and +7% of the prescribed dose. Whilst it is generally accepted that this is not possible for TBI , the effect on the clinical outcome is not known. (Galvin, 1980; Vollans, 2000) Typically ±10% of the prescribed dose to the whole body provides clinically acceptable dose uniformity, with the possible exception of the extremities and other non-critical structures. (Khan, 2003)

Prescriptions tend to be in the range of 5 to 14 Gy, in up to 8 fractions, often treated twice daily. TBI reduces the number of malignant stem cells by a factor of 10 for each 1.5 to 2 Gy. (Quast, 1987) ICRU 29 recommends a prescription point as being central and at a depth of half the patient's thickness. The prescription point when used will typically be in the abdominal or pelvis region (Sanchez-Doblano, 1995), such as the midpoint at the umbilicus level (Syh, 1992). Sometimes the prescription will be to the entire midline or midplane. (Kim, 1980) Sometimes a lower dose rate of 5 – 10 cGy per minute at the prescription point is used. (AAPM report 17)

Radiation dose rate and fractionation schedule can affect the incidence of radiation pneumonitis and need to be considered in the prescription. (Yuille, 1983) Dose limits are sometimes prescribed to critical organs such as the lungs, for example, 9.6 Gy to the lungs when the whole body doseprescription was 12 Gy. (Sanchez-Doblano, 1995, Svahn-Tapper, 1990))

Most data for radiation syndromes come from nuclear incidents and are therefore from a single exposure. For TBI the patient will suffer from bone marrow (or hemopoietic) syndrome. The dose should however be low enough to not cause any concern regarding gastrointestinal or central nervous system syndromes. Following a TBI treatment, patients can survive only if they receive a BMT.

TBI Delivery Techniques

There is no generally accepted technique for delivering TBI. Factors that may influence the way in which TBI patients are treated include the size of the treatment room, energy of the linear accelerator and availability of another linear accelerator as a back up machine. Some centres have dedicated large field TBI irradiators in specially designed treatment rooms but most use standard radiotherapy accelerators for TBI. (Curran, 1989; Podgorsak, 1985; AAPM report 17) Some use single sources of radiation, others dual (Obcemea, 1992) or multiple sources from different directions (Sanchez-Doblano, 1995, AAPM report 17).

If using a single radiation source, such as one accelerator in a bunker, either 2 field or 4 field techniques have been used to deliver TBI (Vollans, 2000). For the two field techniques, they can be either opposed bilateral or anterior/posterior. Anterior/posterior treatments are delivered with the patient in a sitting or standing position (Harden, 2001) or lying on their side. For bilateral techniques the patient is usually supine either lying flat or semi-reclined, often with legs flexed to reduce the patient's length to fit in the field. Four field techniques involve anterior, posterior and bilateral fields. Diagram 2.1 shows some of the delivery techniques used for TBI.

TBI requires the use of a very large, uniform high-energy photon beam so the entire body receives a uniform dose. To get such a large field size, the principle of geometric beam divergence from the source is applied. In order to get a treatment field large enough to treat the entire body, source to axis distances (SADs) of 3 – 5 m are used. (Thomas, 1990)

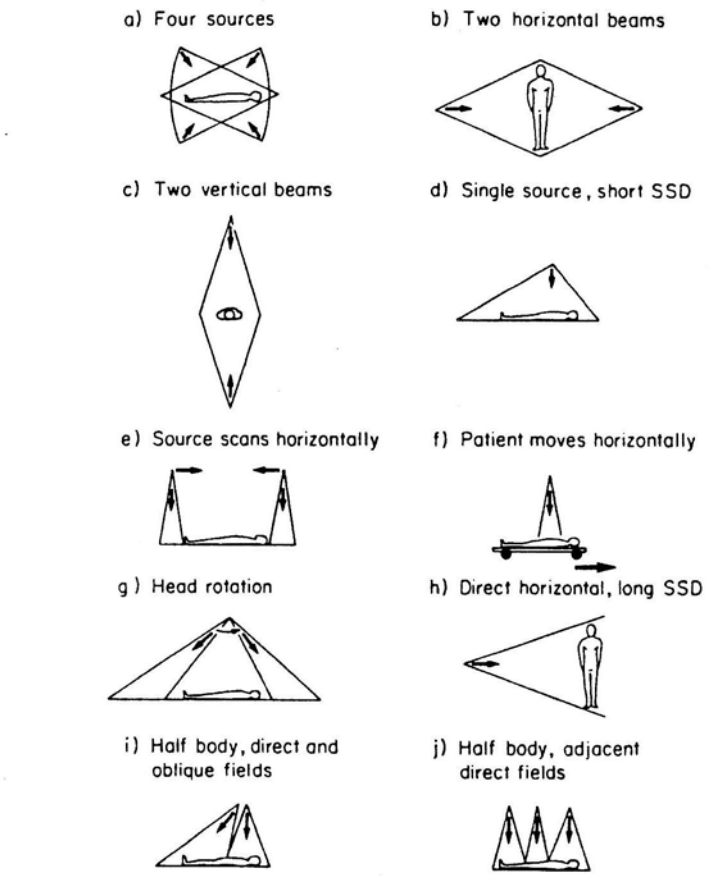

Diagram 2.1 – Shows some of the delivery techniques available for TBI. (Sourced from AAPM report 17)

Various different photon energies are used for TBI, from gamma rays from a cobalt-60 teletherapy units (1.25 MeV) through to linear accelerator beams from 4 MV to 25 MV. (Sanchez-Doblano, 1995) Cobalt-60 Teletherapy units are no longer used for radiotherapy treatment delivery in Australia. For lateral treatments higher energies (ie 10 MV or higher) are preferred for delivering a more uniform dose distribution as the beam needs to travel through the pelvis and shoulder regions. However, for AP/PA treatments, 6 MV beams provide less undesirable high dose regions in the lungs. (Ekstrand, 1997)

Linear accelerators use high frequency electromagnetic waves to accelerate electrons through a linear accelerating tube. To produce an x-ray photon beam these electrons hit a target made of a high Z material such as tungsten, producing bremsstrahlung x-rays. Following the target, the beam intensity is modified by a flattening filter. The target is thick enough to absorb most of the electrons. The beam

then passes through two independent ion chambers, which monitor beam output and symmetry. Finally the beam is collimated.

There are also other techniques that use multiple parallel and adjacent beams or moving beams or patient translation. (Sanchez-Doblano, 1995) These are often applied if a smaller treatment distance is available. Adjacent beams from a single accelerator, such as in diagram 2.1j, create concerns regarding complex dosimetry at field junctions and circulating cells potentially receiving a reduced dose. Using field junctions can also cause concern of hot spots if the beam overlap at the junction or cold spots if there is a gap at the junction. (Rider, 1983)

To achieve a treatment field 2 m long an SAD of 5 m is required. To ensure the patient remains in the field the collimator is rotated through 45° with the jaws opened to the maximum aperture (usually 40 x 40 cm at 100 cm SAD). (Harden, 2001) The TBI treatment SAD can be marked with a laser line which can be aligned to patient midline to aid setup to treatment SAD. (Svahn-Tapper, 1990)

A low atomic number absorber (such as a Perspex^{TM} screen) is often placed in front of the patient, acting as a beam spoiler. This reduces the dose build up region. This improves the dose distribution to the skin, making it more similar to the prescribed dose. For a 10 mm spoiler placed 15 cm in front of the patient with a beam spoiler correction factor applied at a depth of 5 cm, the depth dose increased by only 1% at 2 cm depth. At larger depths the spoiler was found not to influence the depth dose values. (Svahn-Tapper, 1990) The surface dose also increases as beam energy decreases, the distance between the spoiler and the patient decreases and with increasing spoiler thickness (towards depth dose max). A 1 cm thick Perspex^{TM} beam spoiler for a 10 MV photon beam will increase the skin dose up to 97% of d_{max}. (Sanchez-Nieto, 1997) The required thickness of the beam spoiler is dependent upon the energy of the beam, as the position of the d_{max} changes with beam energy. However the clinical effects of skin dose is not known as no systematic study has been completed analysing this. (Kim, 1980)

Tissue Compensation

Some centres do not use any compensation for irregularities in patient shape. (Vollans, 2000) If missing tissue due to contour variations of the patient is to be accounted for, this can be achieved using either missing tissue compensators or tissue-equivalent bolus. These compensators provide greater dose uniformity along the body by reducing the irregularity of the body thickness. (Khan, 2003; Galvin, 1980; Khan, 1980. The compensators are placed between the source and the patient, either in the accessory mount or are mounted onto the beam spoiler.

Bolus material placed around the patient for TBI needs to be malleable and be able to hold a shape at room temperature, as well having a density that is soft tissue equivalent. Strictly this refers to electron density, but physical density can be used satisfactorily as an approximate measure of electron density for low Z materials. Materials such as rice or bicarbonate soda are not quite as dense as tissue (AAPM report 17) but in small bags make suitable bolus materials, although it can be hard to control the thickness. One group designed bolus by making a compound of soft paraffin and acrylic granules, sealed in thin elastic polyurethane bags. This then has a putty type consistency. (Doughty, 1987) Various commercial tissue equivalent bolus materials are also available. Bolus material can also be added under the legs where it not only provides extra scatter but also provides support for the patient. (Yuille, 1983) Missing tissue compensators of lead or copper can also be designed. (Galvin, 1980) The position of the compensators can be verified with film. (Quast, 1987)

Beam Data

Treatment planning systems require beam data to be measured and inputted in order to calculate the dose distributions for treatments. Consideration needs to be given to the different geometry and scatter conditions for TBI when the beam data measurements are being made. It may not be acceptable to simply extrapolate small field data or data measured at isocentre. When using an ion chamber for beam data measurements, care should be taken regarding cable and stem irradiation effects, as the radiation field can cause extra current to be induced in the cable, changing the measured current. This is of particular concern in TBI due to the large field sizes

used which can mean larger lengths of cable being irradiated during measurements. (Fiorino, 2000).

Most linear accelerator monitor unit ion chambers are absolutely calibrated to provide a machine output of 1.0 cGy/monitor unit at machine isocentre under reference conditions. Absolute calibration is done following certain protocols such as the IAEA TRS 398, traceable back to primary standards. For the IAEA TRS 398 protocol, the reference conditions for 6 MV photon beams are to use water as the phantom material, a cylindrical ionization chamber with the reference point on the central axis of the chamber, a measurement depth of 10 g cm^{-1}, a source to chamber distance of 100 cm and a field size of 10 cm x 10 cm. However, some centres use the dose rate or an output factor at the extended SAD for treatment planning for TBI (Abraham, 2000). Dose is defined as “the energy absorbed from ionizing radiation per unit mass” and has the unit of Gray (Gy). (Johns, 1983)

Output factors can be measured to determine the monitor units for extended distances. This would require variations based on patient size and could be used to calculate Tissue Phantom Ratios (TPR) and/or Tissue Maximum Ratios (TMRs). However, as discussed below TMR values vary less than 1.5% for the extended SSD compared to isocentric treatments so dose rate calibrations can also be transferred to extended TBI SSDs. (Khan, 1994)

A TPR is defined as the ratio of absorbed dose at any given depth to the dose at the same point at a fixed reference depth, achieved by changing the source to surface distance. A TMR is defined the same way as TPR except the reference depth is the depth of maximum dose. The setup arrangement for measurements of TMR and TPR are shown in diagram 2.2.

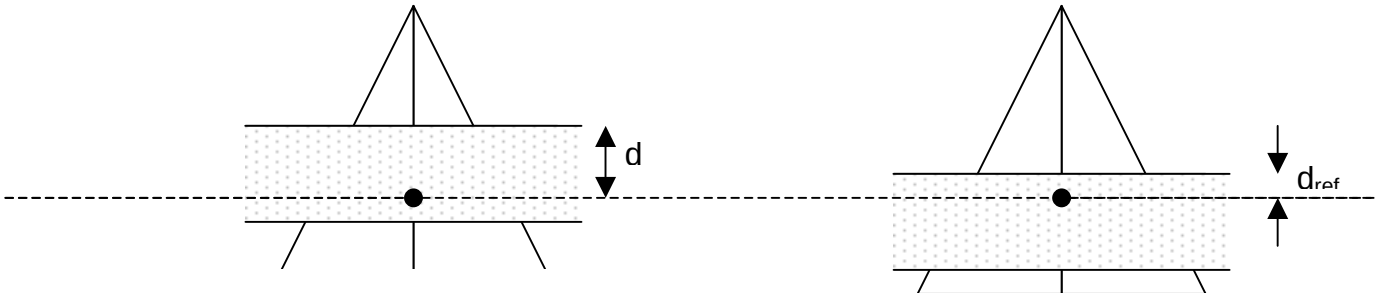

Diagram 2.2 – Setup arrangement for measurement of TPR and TMR, where d is any given depth and d_{ref} is a fixed reference depth for TPR measurements and d_{max} for TMR measurements.

Output factors at extended distance have been measured and the largest difference between the smallest phantom (20 x 20 cm) and largest “infinite” phantom (50 x 140 cm) was found to be 2.4% for a 6 MV beam, implying the phantom size within the large radiation field has a minimum effect on dose rate at the reference point. (Podgorsak, 1985)

TBI requires a beam that covers the entire patient with an adequately flat, uniform beam. As the collimator is often rotated to 45° for TBI the profile is that of a diagonal, which may also affect beam flatness. The TBI beam profile in the gun-target direction should be measured in air, as it is the primary radiation component that is to be measured, not scattered radiation. The beam uniformity decreases as SAD increases. The useful treatment field is that which is within the 94% isodose curve (Sanchez-Nieto, 1997). The dose profile may also include backscattered radiation from the wall.

Varian Linear Accelerators come with flattening filter, which is a cone shaped attenuator. This filter is designed to produce optimal flatness at 10 cm depth for 100 cm SSD. For shallower depths and along the beam diagonals, there will be an overflattening affect, seen as “horns” on a beam profile. For TBI, these horns will be over the body extremities, (head and feet) which may results in some dose enhancements in these areas. This problem was reduced at one institution by the addition of an extra TBI flattening filter. (Doughty, 1987)

Dose ratio data such as Percentage Depth Dose (PDD), TPR or TMR data should be measured at the centre axis and at various off axis points, such as at the level of the

lungs. PDD data varies with patient thickness due to changes in backscatter (Abraham, 2000, Sanchez-Nieto, 1993, Podgorsak, 1985). The PDD can be corrected using a Backscatter Correction Factor (BCF) and Lateral Scatter Correction Factor (LCF). The BCF corrects for lack of backscatter by applying a ratio of the PDD with limited backscatter versus the PDD at the same point if there was infinite backscatter. Hence as backscatter thickness increases towards an infinite thickness, the exponential increase in backscatter tends to 1, due its definition. However, the BCF is linear for depth as the probability of backscatter increases with the depth of the point of measurement.

For TBI treatments close to the bunker wall, back scattered radiation from the wall as well the patient can be seen. For smaller phantoms midline dose will be influenced more by backscattered radiation from the wall than for larger phantoms, which should be considered when choosing a phantom. (Svahn-Tapper, 1990)

Similarly the LCF is the ratio between a PDD at a certain point for a given cross section versus the PDD at the point for an infinite cross section giving full lateral scatter. As with the BCF, the LCF has linear variation with depth and exponential variation with distance to lateral surfaces, which tends to 1 as the thickness tends towards full lateral scatter conditions (ie almost infinite distances to the lateral surface, providing almost infinite lateral scatter).

As the SAD increases, the PDD shifts due to the inverse square law (Metcalfe, 1997). Not considering the deviation from the Inverse Square Law (ISL) due to changed scatter conditions, the PDD at extended distances can be approximated using the Mayneord Factor. (AAPM report 17, Mayneord 1994) Data calculated from 100 cm SSD data using the Mayneord factor has been compared to SSD data measured at TBI treatment SSD (in this case 455 cm) with TBI scatter conditions. The measured and calculated data agreed to within 2.5% for several depths from 5 cm to 30 cm. (Sanchez-Nieto, 1993) This error can be as large as 6%. (AAPM report 17) Therefore measurements should be made to confirm any conversions if needed in large beam geometry at treatment SSD.

Off axis TMR measurements can be normalised to central axis TMR measurements. It has been found that for TMR 35 cm and 70 cm off axis the difference between

central axis and off axis TMRs are 1% and 4-5% respectively for large depths. (Svahn-Tapper, 1990) This is due to changes in the energy spectrum across the beam. For TBI this means that central axis TMR measurements are not valid in the distal head and feet regions.

Collimator scatter factors (CSF) correct for the difference between the field size at calibration (typically 10 cm x 10 cm) with the treatment field size, due to changes in scatter within the linear accelerator head. The collimator scatter factor at TBI SSD should not vary much compared to the data measured at isocentre. The data at the two distances for field sizes larger than 25 cm x 25 cm has been found to be within 0.3% with up to 1% variation for field sizes of 10 cm x 10 cm. (Smith, 1996, Curran, 1989) Because the jaws are always set to 40 cm x 40 cm for TBI, this will not vary significantly between the two distances. CSF can be measured with an ion chamber in air with a cylindrical build up cap providing a build-up depth for the photon energy being used.

The peak scatter factor (PSF) corrects for changes in the phantom for the treatment field size as compared to the 10 cm x 10 cm field used for calibration. For conventional radiotherapy, the phantoms used to measure the data are normally larger than the radiation field. However, for TBI this is not the case, but rather the phantom is significantly smaller then the radiation field. This may affect the TMR and PSF values for TBI. The changes for PSF depend on energy but will vary less then 1%. The TMRs have been found to vary by less 1.5%. (Curran, 1989, Khan, 1980)

Due to scattered radiation from the bunker walls, floor and linear accelerator head, discrepancies may be seen if the ISL is used to calculate the dose rate at the TBI treatment SAD. (AAPM report 17, Rider, 1983, Van Dyk, 1987) The deviation between the inverse square law and measured data increases with distance from the reference. This deviation from the ISL can be fitted as a four-order polynomial, with an error between measured and calculated data of less than 0.08%. (Sanchez-Nieto, 1997) This must also be considered in terms of the different source to point distances within the body (Sanchez-Doblano, 1995). Other investigations have shown no systematic deviation from the inverse square law when it is measured on the central axis at various depths in a 30 cm^3 phantom at SSD of 430 cm. (Svahn-Tapper, 1990) Other investigations found that the inverse square predicted the measured dose to

within 1.5% for a variety of energies and distances. (Curran, 1989) However deviations of up to 6% have been reported (Quast, 1987).

For TBI treatments, the equivalent square of the frontal side of the patient (from the beam's eye view) should be used for the field size when calculating the TMR and PSF values as opposed to the jaw opening size. (Curran, 1989) This is because the field size is larger then the scattering volume. This is particularly important for TMR. The area over perimeter method is an adequate method for calculating the equivalent square for TBI. (Podgorsak, 1985) Ideally when beam data measurements are being made the phantom should be of similar equivalent square size to the patient so that errors can be minimised. (Kirby, 1988)

Treatment Planning

Currently there is no commercially available treatment planning system for TBI. Planning for TBI typically entails calculating at least one point dose. The total dose at any point is the sum of the primary beam plus scattered radiation.

For manual calculations, the thickness of the body in the beam direction needs to be determined at each reference point. This data is available from CT measurements but mechanical measurements are an alternative. (Quast, 1987) An effective depth that corrects for tissue density heterogeneities can also be used in manual calculations. This is especially important for points near the lungs.

Some centres have also developed in house TBI treatment planning systems, using x-ray computed tomography (CT) data. (Sanchez-Nieto, 1997) CT scans provide anatomical information as well as density heterogeneity information. Considering the patient's physical parameters and anatomy can optimise the dose distribution in the patient. (De Sapio, 1990, Quast, 1986).

To use the density heterogeneity information from a CT scan, the CT numbers need to be calibrated to physical electron densities using an electron density calibration phantom. Radiotherapy treatment planning systems use data tables to assign an electron density to each pixel's CT number or Hounsfield Unit, which is based on the gray scale. (Khan 2003)

However, since at the megavoltage energies used for radiotherapy the Compton effect is the dominant photon interaction, it is the electron density (number of electrons per cm^3 multiplied by mass density) of a material that has the most effect on beam attenuation. However, since the number of electrons per gram of material is very similar for many materials, (Khan, 1994) the mass density of a material may also be used for calculating the heterogeneity corrections.

There are different methods for correcting for tissue density heterogeneities. These methods vary from simple corrections that only correct for changes in the fluence of the primary photon beam through to convolution methods, which also account for scattered radiation and electron transport. Monte Carlo simulations are the most accurate method but require long computational periods that are currently impractical.

The effective depth can be calculated by multiplying assumed heterogeneity correction factors for lungs by the patient's measurements for planning purposes. (Vollans, 2000)

$$d_{eff} = d - (\rho_{rel\ lung} \times d_{lung}) \quad (1)$$

Where d_{eff} is the effective depth

d is the physical depth

$\rho_{rel\ lung}$ is the relative density of the lung tissue

d_{lung} is the physical depth taken by lung tissue

Lung density can vary between 0.15 g/cc to 0.4 g/cc as compared to water at 1.0 g/cc so heterogeneity corrections are important. By studying layered lung geometry another investigator has found that for lung density 0.31 g/cc, a lung correction factor of about 1.5% per centimetre of lung tissue has been found to be necessary, and that this holds for both calculations and measurements. (Obcemea, 1992)

Another method uses a ratio of TARs for the physical and effective depths. (Metcalfe, 1997) This method does not take into account the relative position of the inhomogeneity, the lateral extent of the structure or electron transport. (El-Khatib, 1986)

The Batho power law method uses TARs raised to an exponent, which depends on tissue density. Batho originally introduced this method for calculating doses beyond a single inhomogeneity. (Batho, 1964) This method was then extended to include doses within the inhomogeneity (Sontag, 1991) and to calculate for a number of inhomogeneities (Webb, 1979). This algorithm implicitly considers scattered radiation. (Metcalfe, 1997) This method considers the relative position of the structure. (El-Khatib, 1986) It can account for the lateral extent of the inhomogeneity if scatter summation is also applied. (El-Khatib, 1986, Lulu, 1982) It does not consider secondary electron transport. (El-Khatib, 1986)

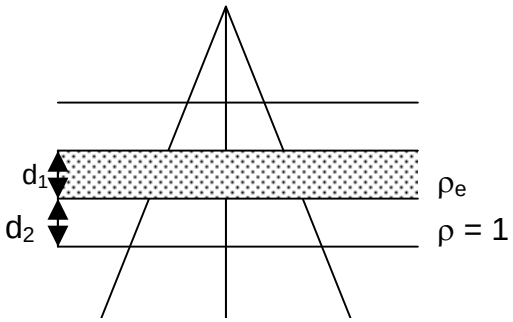

Diagram 2.3 – Setup for Batho density correction.

$$CF = \left[\frac{TAR(d_1 + d_2, f)}{TAR(d_2, f)} \right]^{\rho_e^{-1}} \qquad (2)$$

Where CF is the correction factor

d_1 and d_2 are the depths are shown in diagram 2.3

f is the field size

ρ_e is the density of the lung tissue

For a single layered heterogeneity with a less than unit density, the dose is underestimated within the low density region, with the largest errors near the top of the heterogeneity. However the method shows good experimental agreement below the heterogeneity. This method generally works well for smaller fields but the larger the field the larger the error, due to the increase in scatter affecting the percentage depth dose curve. (Metcalfe, 1997)

The equivalent TAR method uses multi slice CT information to account for scattered radiation. It uses ratios of TARs depending on effective beam radius (to account for scattered radiation) and effective depth (correcting for primary beam). (Metcalfe, 1997) This method considers the relative position of the inhomogeneity and the lateral extent of the inhomogeneity but does not consider secondary electron transport. (El-Khatib, 1986) In comparison with measured data (when the field is large enough for electronic equilibrium) this method gives accurate results, which implies that it adequately models scatter dose. (Metcalfe, 1997)

The differential Scatter-Air Ratio method takes the primary dose and then adds scatter radiation. The scatter can be calculated either assuming homogeneity or correcting for heterogeneity by considering the attenuation of the primary beam for each scatter element or including the attenuation of scattered photons in their path to the calculation site. (Metcalfe, 1997) This method considers the relative position of the inhomogeneity and the lateral extent of the inhomogeneity but does not consider secondary electron transport. (El-Khatib, 1986) A similar method is the delta volume method. (Metcalfe, 1997)

Although these methods can calculate the effect of inhomogeneities on photon fluence they cannot predict changes to secondary electron transport. However, when electronic equilibrium exists, electron transport can be ignored. Therefore, when electronic equilibrium exists these methods are more accurate as the change in dose is proportional to primary photon fluence. (Metcalfe, 1997)

Computerised planning systems used for non-TBI radiotherapy planning can assist in TBI treatment planning, including calculating lung inhomogeneity corrections. The

two types of computer system used in this project are based on the 2D Bentley – Milan algorithm (Milan, 1974) with modified Batho inhomogeneity corrections (Radplan^{TM}) and 3D convolution model (Pinnacle^{TM}, ADAC Laboratories, Milpitas CA).

The Bentley – Milan algorithm for dose calculation accounts for patient contour variations and different SSDs. (Milan, 1974; Storchi, 1996; Metcalfe, 1997) The algorithm makes use of measured central axis PDD and beam profiles. The beam data is measured for different square field sizes and profiles are measured at different depths.

The beam data is entered into the computer as 47 fanlines. The central fanline, on central axis, contains 17 PDD points. There are then 23 fanlines off axis on each side of the central fanline. The profiles are normalised to 1.0 on the central axis and then multiplied by the PDD value at the depth of the profile. Thus the fanline grid gives information regarding the increasing geometrical penumbra with depth and changes to the scatter dose. The algorithm interpolates within the fanline grid for dose calculation.

The general Bentley – Milan algorithm is:

$$D(d, y, f_2) = PDD\left(\frac{SSD_1 + d}{SSD_1 + d_{\max}}\right)^2 R(d, y', f_1)\left(\frac{SSD_1 + d_{\max}}{SSD_2 + d}\right)^2 \qquad (3)$$

Where D is the dose

d is the depth

R is the off axis ratio

y is the off-axis distance

f is the field size

y' is the projected off axis distance at the reference SSD for patient contour variations.

Investigations have been completed to evaluate using the ADAC Pinnacle^{TM} treatment planning system for TBI planning. (Abraham, 2000) This paper first investigated the heterogeneity corrections calculated by Pinnacle^{TM} at the isocentre level (100 cm SAD). This was completed by comparing film dosimetry with calculated data. They then placed the RANDO^{TM} anthropomorphic phantom at the extended SSD for TBI set-ups and exposed two films and compared these films to the calculations from Pinnacle^{TM}.

Diagram 2.5 shows the basic geometry used for a convolution method. Convolution methods involve two components: TERMA, which represents the total energy imparted into the medium by interactions of primary photons and a kernel, which represents energy deposited around a primary interaction site at vectorial displacements, as a fraction of TERMA. (Metcalfe, 1997)

TERMA is an acronym for total energy released per unit mass by an ionising particle. It includes the energy from both secondary charged particles and scattered photon energy, which is the same as the energy of the incident photon. Thus TERMA is the energy lost from the primary beam per unit mass.

Kernels can be obtained from Monte Carlo simulations and show the pattern of energy deposition within an array of voxels. Kernels are comprised of either two or three components. Firstly there is the primary component for the primary dose and then either a scatter component (for first and multiple scatters) or a first scatter component and then a multiple scatter component. Because kernels vary in inhomogeneous media this is not strictly convolution but superposition. Kernels also account for the change in the transport of scattered radiation due to inhomogeneities. Diagram 2.4 shows an energy deposition kernel.

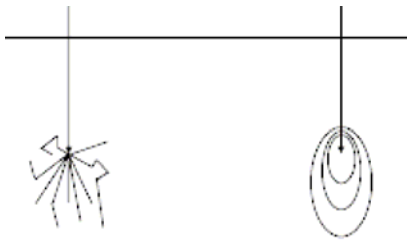

Diagram 2.4 – Energy deposition kernels

The collapsed cone convolution method uses an analytical kernel represented by a set of cones. The energy deposited from each of these cones is collapsed onto the central ray line of each cone, hence it is the collapsed cone convolution method. (Butson, 2000)

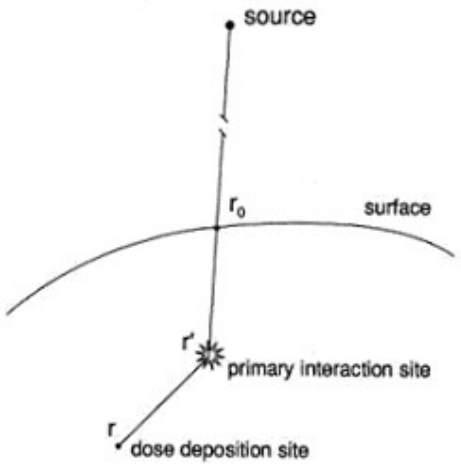

Diagram 2.5 – Shows the geometry for convolution calculation methods. (sourced from Metcalfe, Kron and Hoban, 1997)

If the energy fluence of primary photons at point r' is $\Psi(r')$ then TERMA T(r') is given by:

$$T(r') = \frac{\mu}{\rho}(r')\Psi(r') \quad (4)$$

where $\frac{\mu}{\rho}$ is the mass attenuation coefficient.

For polyenergetic beams the equation needs to be modified to include each energy component in the beam spectrum:

$$T(r') = \sum_{n=1}^{N} \Psi_n(r') \left(\frac{\mu}{\rho} \right)_n \quad (5)$$

Where n is a component of the energy spectrum.

For each point in a unit of mass the attenuation due to the change in depth from the surface will be different. :

$$T(r') = \left(\frac{|r_0|}{|r'|} \right)^2 \sum_{n=1}^{N} \Psi_n(r_0) e^{-\mu_n |r' - r_0|} \left(\frac{\mu}{\rho} \right)_n \quad (6)$$

Where $|r'-r_0|$ is the geometric depth to point r'.

For an inhomogeneous medium the effective depth needs to be used rather then the geometric depth. For divergent beams the inverse square law falloff must also be considered.

In the convolution/superposition process, each kernel is modulated by the TERMA to obtain the dose at each point. For a homogeneous medium:

$$D(r) = \int_{r'} T(r') \left[H_p(r - r') + H_s(r - r') \right] d^3 r \quad (7)$$

For an inhomogeneous medium:

$$D(r) = \frac{1}{\rho(r)} \int_{r'} T(r') \rho(r') \left[H_p(r', r - r') + H_s(r', r - r') \right] d^3 r \quad (8)$$

NB: For homogeneous media, $\rho(r) = \rho(r')$ and therefore these terms cancel out.

For calculation between two points, an average density along the path length can be found, creating an effective path length. This can then be used for calculation of the energy loss of secondary electrons travelling from r to r'.

$$\rho_{ave} = \frac{1}{|r - r'|} \int_{r'}^{r} \rho(r'')dr'' \quad (9)$$

This is not strictly correct because electron scattering depends not only on average density but also the density distribution but the average density works as an approximation.

$$D(r) = \int_{r'} T(r') \frac{\rho(r')}{\rho_{ave}} \left[H_p(\rho_{ave}, r - r') + H_s(\rho_{ave}, r - r') \right] d^3r \quad (10)$$

In order to save calculation time where the kernels are spatially invariant, the convolution/superposition process can be performed in Fourier space.

$$D = T \otimes K \quad (11)$$

Where: D is the dose
T is the TERMA
K is the kernel.

$$\Im(D) = \Im(T) \times \Im(K) \quad (12)$$

The dose is therefore obtained from the inverse Fourier transform of the convolution/superposition performed in Fourier space.

In Pinnacle^{TM} both the collapsed cone convolution and adaptive convolution dose calculation engines use the same algorithm. For adaptive convolution varying the resolution of the dose grid based on a dose gradient difference method, thus decreasing the calculation time.

The ADAC Pinnacle^{TM} treatment planning system uses a three-dimensional collapsed cone convolution algorithm to calculate dose. It can calculate the effects of

patient heterogeneity for both primary and scattered radiation, even in areas of perturbed electronic equilibrium, such as tissue air interfaces. This is important for lung dose modelling.

For a slab phantom (solid water/lung/solid water) it has been found that data calculated from the Pinnacle^{TM} TPS and measured data agree within 2% for a field size of 5 x 5 cm, at 6 and 10 MV. The method overestimates the dose just beyond the lung tissue interface due to charged particles being more laterally deflected than predicted by the kernel density scaling method. (Butson, 2000)

Dose Distributions

For megavoltage beams used for TBI there is a predominance of Compton interactions (Khan, 1994), which are almost independent of effective atomic number, but vary with effective electron density. Hence it can be assumed that the presence of an inhomogeneity modifies the photon fluence but not the absorption processes. (Sanchez-Nieto, 1997)

For bilateral treatments, the dose uniformity across the patient will be higher for higher energy beams as they will penetrate further. Also, increasing the SAD causes less dose variation across the patient. For AP/PA treatments with patient separation between 18 and 26 cm most megavoltage treatments will provide dose uniformity across the patient within 15%. There will be high non-uniformity for bilateral treatments. (AAPM report 17)

The dose distribution may be less uniform for bilateral techniques than the AP/PA techniques, especially for larger patients and lower energies, (Syh, 1992) but it can be more comfortable for the patient to be able to lie flat for bilateral techniques.

For a four field technique, it has been found that a more homogeneous dose distribution will be achieved if approximately two-thirds of the dose is delivered from the anterior/posterior fields with the remaining third coming from the lateral fields (Cosset, 1994).

Lung Doses

Within the lungs (compared to soft tissue) there is decreased attenuation of photons and a loss of scatter (increased ratio of primary to scattered radiation) and, as scattered radiation has an increased range, electronic disequilibrium, which results in a loss of dose. This effect increases for smaller field sizes and higher energies. Due to the higher proportion of primary radiation leaving the lungs, there is an increased dose build-up on the exit side of the lungs. (Khan, 2003)

Lung tissue is both radiation sensitive and responsible for many of the potential fatal side effects from TBI, this includes radiation pneumonitis. Hence the lung is the main critical organ at risk in TBI. The probability of radiation pneumonitis depends on the volume of lung irradiated and total dose. A 5% change in lung dose could result in a 20% change to the probability of a patient developing radiation pneumonitis. (AAPM report 17)

Thus the lung dose is important, and lungs are often shielded during TBI treatments, especially if the prescribed dose is above lung tolerance. During most lateral TBI treatments, the patients will lie with their arms beside them, partially shielding the lungs.

Many parameters influence the dose received to the lungs. These factors include anatomical factors such as lung size, density and position in the body, position of the calculation point and beam quality. (Quast, 1987)

To reduce lung doses, customised lead, cerrobend (bismuth 50%, lead 26%, tin 13% and cadmium 11%) or rose metal (bismuth 50%, tin 25% and lead 25%) compensators can be used as filters (Harden, 2001, Sanchez-Nieto, 1997, Svahn-Tapper, 1990). These compensators can be supported on Perspex^{TM} beam spoiler screens and can be designed from thoracic radiographs taken with the patient in treatment position. Portal films can be taken to confirm location of the compensators. If blocks are mounted on the accessory mount rather then on the Perspex^{TM} beam spoiler the principle of geometric divergence means that blocks can be made much smaller then the organs they are required to protect. However, care should be taken

regarding the penumbra around such blocks if they are mounted too far from the patient. The compensators can be either present for the entire treatment or just part of the treatment.

Compensators can also be designed by calculating the monitor units and dose to several different points in the body and then adding layers of lead to make these more uniform (Quast, 1986).

If a bilateral technique is used and lung shielding is employed, it should be noted that this would reduce the dose to the mediastinum, as this will also be shielded.

Partial transmission shields may also be used to reduce the lung dose without completely shielding them, thus also giving dose to the mediastinum. A similar technique involves using shielding blocks for only part of the treatment time. (Khan, 1994)

Dose Verification - Phantom Measurements

Dose distribution data can be measured using a phantom. A phantom is a term that refers to a material that simulates the radiation absorption and scattering properties of the tissue of interest. Simple phantoms are composed of water, which has similar radiation absorption properties to muscle and other soft tissues. Other solid materials have also been developed with the similar electron density for water for use as phantoms in the megavoltage range. (Khan, 2003)

Treatment planning techniques can be evaluated using an anthropomorphic phantom. The phantom simulates the patient and can be CT scanned for accurate treatment planning. A commercially available anthropomorphic phantom is the RANDO^{TM} phantom produced by the Alderson Research Laboratories, Inc. in Stamford, Connecticut. This phantom incorporates materials to simulate tissues such as muscle, bone, air cavities and lungs, with a similar contour to a typical head, neck and torso. (Khan, 2003)

These phantoms allow for close positioning of TLDs and also allow slots for films. This allows for dose distributions to be obtained and compared to plans, without

distortions from changes in anatomy, but with anatomy that is representative of a real patient. Effective organ doses can also be calculated from this data. (Syh, 1992)

For cases where a “standard” patient size is not representative, another humanoid phantom technique has been posed where water containers are laid out and filled with water to different heights to represent patient thickness at each site (Obcemea, 1992).

Dose Verification – Invivo Dosimetry

Due to the complex calculations required to obtain dose distributions and their inherent difficulties, combined with clinical issues such as patient movement, invivo dosimetry is the optimal way to check the actual dose delivered to the patient (ICRU report 24, 1976). It is also important to know the dose delivered to a patient accurately for treatment records for comparisons of treatment results, patient statistics and to assess side effects.

Commonly used are semiconductor diodes and MOSFETs, ion chambers and Lithium Fluoride (LiF) TLDs. These are used to measure exit and entrance doses. Depending on the type of dosimeter, the temperature of the dosimeter may need to be considered (ie closer to body temperature than room temperature and time for the dosimeter to reach thermal equilibrium).

The electrical safety of high voltage dosemeters such as ion chambers also needs to be considered during TBI treatments. It is also preferable to have real time results, also provided by diodes and mosfets.

The detectors used for invivo dosimetry need to be correctly calibrated and commissioned prior to use to ensure optimised reproducibility and accuracy is achieved.

Dosimetry data from invivo dosimetry can then be used to modify the number of monitor units given per fraction. At some centres (Harden, 2001) the number of

monitor units given for the first fraction is standard and the number of monitor units for each other fractions is determined only from the results of the invivo dosimetry. The dosimetry data can also be used to vary lung compensator lead thickness if required to ensure lung is adequately shielded.

For patients smaller then about 20 cm thickness, an average of the entrance and exit doses will give a midline dose with an accuracy of about 1 – 2%. However, for thicker patients, the shape of the depth dose curves must be considered to obtain an estimate of the midline dose to the patient. (AAPM report 17)

The dosimeters may measure entrance and exit doses. Dosimeters can also be placed along the midline of the patient, eg, between the legs, to determine midline dose. Doses to areas where body thickness varies, such as the feet, head and neck can be assessed with invivo dosimetry. Dosimeters around the axillae can assess the lateral dose uniformity and aid in assessing lung dose. (AAPM report 17)

Thermolumniscient Dosimetry

Certain crystalline materials such as lithium fluoride absorb x-ray energy by lifting electrons from the valence band to the conduction band and by adding impurities into the crystal these electrons then fall into impurity traps in the forbidden zone between the valence band and the conduction band. The electrons in the impurity traps are storing energy. This energy is then released when sufficient heat is added to lift these trapped electrons back into the conduction band where they can then fall back into the valence band, emitting their excess energy as a visible light photon. This process is known as thermoluminescence. The light emitted is proportional to the x-ray energy absorbed and thus provides a way of measuring absorbed dose. (Bomford and Kunkler, 2003) TLDs are dose rate independent. (ICRU 21)

Preparation for TLD measurements should also include a standard pre-irradiation anneal of 400°C for 1 hour followed by 100°C for 2 hours. The heating cycle for reading the chips should be the same as was used for calibration. Both the reader and each individual chip should be calibrated. (Amor Duch, 1998) The detectors should be surrounded by build up materials to ensure electronic equilibrium.

After being exposed to radiation the TLDs are read in a specialized “reader”. The TLDs are heated to 300°C. The light output is measured using a photomultiplier tube,

which converts visible light into an electrical current which can be amplified and recorded. The thermoluminescence of a material plotted against temperature is called a glow curve. (Bomford and Kunkler, 2003; Kahn, 2003)

TLDs are a relative dosimeter and require calibration by comparison with other TLDs exposed to known doses of radiation of the same quality. (Bomford and Kunkler, 2003)

Lithium Fluoride has an effective atomic number of 8.2, which is similar to that of soft tissue which has an effective atomic number of 7.4. Lithium Fluoride is almost independent of energy in the range typically used in a radiotherapy department. (Bomford and Kunkler, 2003)

Film Dosimetry

Radiographic film has a cellulose or polyester base coated with an emulsion containing silver bromide crystals doped with silver sulphide to make the crystal lattice sensitive to visible light and x-ray photons. (Bomford and Kunkler, 2003)

When exposed to radiation, the crystal emulsion undergoes chemical changes forming a latent image. The film is developed and the affected crystals become smalls grains of metallic silver. During the fixing process, the unaffected crystals are removed, leaving clear film in their place. The metallic granules are not affected by the fixer so stay in place, darkening the film. (Khan, 2003)

The degree of darkening is thus proportional to how much incident radiation there was. So dose is proportional to optical density, OD, defined as:

$$OD = \log I_o/I \quad (13)$$

Where: I_o is the incident light
I is the transmitted light through the film

With excellent spatial resolution and being capable of dose integration, film is suitable dosimeter for practical two dimensional dosimetry. Kodak EDR2 film is

commonly used for radiotherapy dosimetry verification as it can accurately measure high doses without saturating as it has smaller grains and fewer high Z silver halide molecules than other films, reducing its over response to lower energy radiation. (Childress, 2005) Kodak EDR2 film has a linear dose response to about 5 Gy. For comparison, Kodak XV2 film for therapy verification saturates at about 1 Gy so has a very limited linear dose response region. (Dogan 2002) It has been shown to be insensitive to dose rate. (Buciolini, 2004).

Delays between exposing and processing EDR2 film can affect its optical density response by as much as 4 - 6%. The optical density response has stabilised to 99% of its value by one hour. (Childress, 2004).

Chapter Three – Methods

In this chapter I describe how I modified an anthropomorphic phantom. This allowed multiple lung sizes to be simulated and the effect that this would have had on the effective chest width calculation required for TBI planning. The planning process is described, as are the verification techniques.

Phantom design

An anthropomorphic tissue equivalent phantom (RANDO, Alderson labs) was modified for this project so that any effects of lung size could be ascertained. The phantom is comprised of 2.5 cm thick slices as seen in diagram 3.1. The material simulating muscle has a density and effective atomic number similar to muscle so radiation interacts with the material in a similar way to muscle. The lung tissue has a lower density and closely simulates lungs in the median respiratory state. Higher density material is used to simulate the bones.

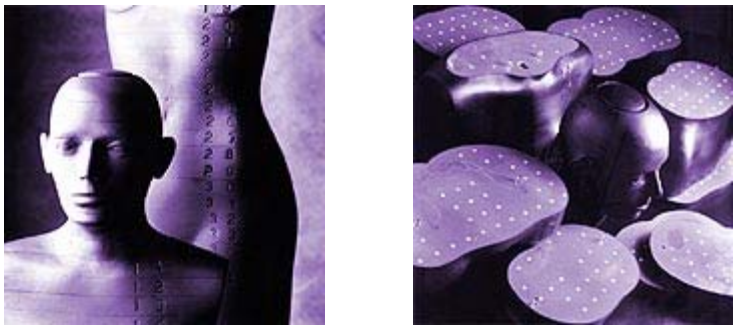

Diagram 3.1 – Shows the RANDO™ phantom, both complete and in sections, including the slots for TLD placement.

The unmodified RANDO™ phantom was CT scanned allowing visualisation of which slices contained low density lung material. All slices containing low density lung material were then replaced with Perspex™ slices of the same size with removable inserts for lungs (cork) of different sizes. This allowed lung lateral dimensions to be varied for the purposes of this study. Perspex™ was used as it simulates muscle tissue. Cork was used as it has a low density similar to lung tissue. (ICRU 44)

In the modified phantom, hereafter described as the RANDO^{TM} lung phantom, there were four sizes of lung. Starting with the largest lung, 1 cm of cork from the lateral surfaces of the lung could be replaced by a 1 cm insert of Perspex^{TM}, providing a narrower lung. Similarly, cork could be removed from the anterior and posterior surfaces of the lung, and replaced with Perspex^{TM} making the lungs shorter. The length of the lungs in the inferior – superior direction could also be changed. Thus four lung sizes (largest lung, smallest lung, wide short lung and narrow tall lung) were made. This can be seen in diagram 3.2.

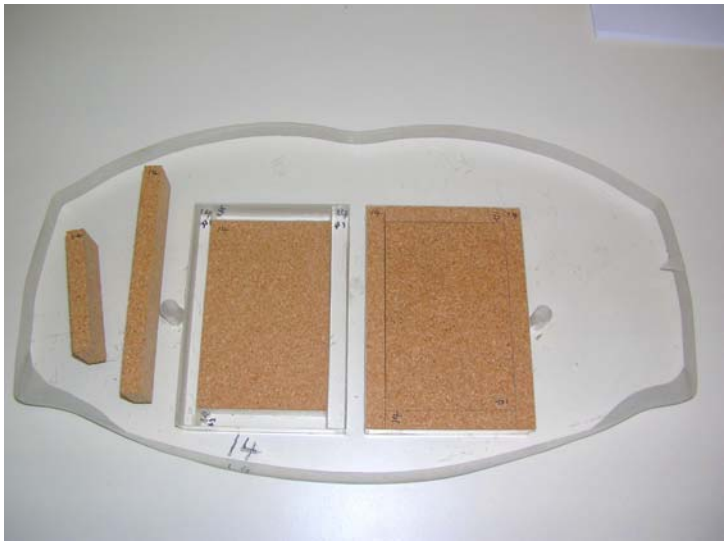

Diagram 3.2 – a slice of the lung insert part of the anthropomorphic phantom modification showing the arrangement of the smallest lung on the left, with a cork insert surrounded by Perspex^{TM} inserts and the largest lung, with the cork insert from the smaller lung arrangement surrounded with cork inserts, as also seen loose on the side.

As the area of interest for the phantom verification testing was not near the surface, for ease of setup a beam spoiler was not used during either planning or treatment.

Measurements of Phantom

The RANDO^{TM} lung phantom was scanned on a clinical GE HiSpeed CT scanner (General Electric Medical Systems, Milwaukee, Wisconsin) dedicated to radiotherapy simulation. The physical chest of the width was determined from the CT scan data and the width of the hip of the RANDO^{TM} lung phantom was measured physically with

callipers. This data is required in the TBI planning process for Monitor Unit calculation.

Scout scans were completed first and the lung area was then selected for the helical scans. The scans were performed using a chest reconstruction algorithm. They were full helical scans, with a pitch of 1, 1 s rotation time and the exposure parameters were 120 kV and 130 mA. The slices were each 2 mm thick.

Prescription

The most common prescription at Westmead is 12 Gy in 6 fractions (2 Gy/fraction) treated bi-daily with at least 6 hours between each fraction. For some paediatric patients the dose rate may also be limited to be below 10 cGy/min at the midplane. Together with a smaller dose per fraction this reduces the risk of radiation pneumonitis, which is a higher risk in paediatric patients. Dose rate control on a linear accelerator can be achieved by varying the continuously variable pulse repetition frequency control.

Planning

Two planning systems, Radplan™ and Pinnacle™ were used to calculate monitor units with heterogeneity corrections turned on and the plan repeated for homogeneous conditions, for both primary and scattered radiation.

Radplan™ is a treatment planning system that uses the Bentley – Milan algorithm to calculate dose and the Batho method to correct for heterogeneities. It uses a sector integration method.

Pinnacle™ (ADAC Laboratories, Milpitas, California) is a commercially available treatment planning system that uses a convolution method to calculate dose distributions for radiotherapy. An adaptive convolution algorithm was used with a dose grid of 0.4cm in all directions. This allows for speed of calculations with no significant effect on accuracy.

Beam Parameters

Two laterally opposed, isocentric and symmetric beams were used. The 6 MV beams are from a Varian 6Ex Clinac (Varian Medical Systems Inc, Palo Alto, California) using the IEC scaling system. (IEC, 2002) The linear accelerator monitor unit ion chamber is absolutely calibrated to provide a machine output of 1.0 cGy/monitor unit at machine isocentre following the IAEA TRS 398 protocol. Table 3.1 shows the parameter settings used for the beams. For Pinnacle^{TM} the isodose distribution was also calculated for a 400 cm SAD.

Parameter	**Settings**
Field size	40 x 40 cm
Collimator angle	45°
Gantry angle	90° and 270°
Couch angle	0°

Table 3.1 – Beam parameters

In the treatment planning systems the treatment was planned at a SAD of 100 cm, as beam data was not available at the extended SAD for TBI. The extended SAD is accounted for in the treatment monitor units by the inverse square law factor.

Point of Interest and Prescription

A point of interest is added and positioned so that is in the middle of lungs and gives an even depth for each beam. The two beams were added with a 50% beam weighting. The plan is then calculated, giving the number of monitor units required to be delivered for each beam so the prescribed dose is delivered.

In Pinnacle^{TM}, the prescription was made to the calculation point and in Radplan^{TM} the prescription was made to the isodose line that that passed through the calculation point.

Repeat Trial for Homogeneous Density Correction

The plan was then repeated but the heterogeneity correction was changed to homogeneous for both primary and scattered radiation. The monitor units and isodoses were recalculated. This simulates a CT dataset with the same external patient contour but with a density of 1 g/cm^3, measuring the effects of the heterogeneity of the lungs.

Isodose Maps

Isodose maps were produced to provide a method for visual evaluation of the dose distribution. The isodose maps are displayed in absolute dose. See diagrams 4.4 – 4.10.

Effective Chest Width and Treatment Monitor Unit Calculation

The monitor units for heterogenous and homogeneous plans from both Radplan™ and Pinnacle™ were then used in conjunction with physical measurements of the chest width and hip width to calculate the treatment monitor units and bolus requirements from data used for standard planning data.

The ratio between monitor units of corresponding heterogeneous and homogeneous plans was used to calculate the effective chest width, by correcting for the heterogeneity caused by the lungs. This is achieved by multiplying the ratio by the TMR for the equivalent square and depth (based on half the measured distance from the left to right axilla). The equivalent square was calculated using the area over perimeter method.

$$\text{Equivalent Square} = \frac{2 \times H \times T}{H + T} \quad (14)$$

Where H = patient height and
T = patient thickness at hips.

Ratio = homogeneous monitor units/heterogeneous monitor units

$$TMR_{(S,\,eff)} = TMR_{(S,\,m)} \text{ x ratio} \quad (15)$$

Where $TMR_{(S,\,eff)}$ = the TMR for the equivalent field size S and the effective depth

$TMR_{(S,\,m)}$ = the TMR for the equivalent field size S and half the measured distance between the left and right axilla.

The effective depth can be found from the TMR tables. Because the point is at midline, doubling his value gives the effective axilla to axilla distance.

The patients lay with their arms beside their chest within the TBI cradle, so the Perspex™ sides of the cradle and the patient's arms need to be included in the

effective chest width used for calculations (this was not the case for RANDO™, as RANDO™ has no arms and for the verification measurements no Perspex™ screen was used). During the initial patient measurements, a chest width measurement is taken, which includes the total chest width. This was corrected using the difference between the measured and effective distance between axillae. The effective chest with is thus calculated:

$$(W_s)_{eff} = W_s - (d - d_{eff}) \quad (16)$$

Where $(W_s)_{eff}$ = the effective chest width

W_s = the measured chest width

d = measured distance between axillae

d_{eff} = effective distance between axillae

As the hip width is always larger than the effective chest width for both phantoms used, the hip width is used to calculate the monitor units for treatment and bolus is placed around the chest for treatment. The extra bolus placed around each side of the chest is half the difference between the hip width and effective chest width.

If the hip width was smaller than the effective chest width the depth used for monitor unit calculation would be half the effective chest width and bolus would be around the patient's hips.

The bolus material used for treatment is small bags filled with rice. Around the head and neck region extra Perspex™ is added to the side of the TBI cradle so the effective width is the of the head is the same of the width used for calculation. Bolus is wrapped around the patient's neck to bring the neck width to the same as the head width.

Half the hip width is thus used as the depth to which the monitor units are calculated, to give the prescribed dose to the midline of the patient. However, for the verification

measurements, the effective chest width was used and no bolus was added as the measurement were taken around the chest region.

The monitor units are calculated using the following formula:

$$MU = \frac{D \times 100 \times PSF(10)}{TMR(P/2, S) \times AAF(x, y) \times PSF(S) \times ISL} \quad (17)$$

Where D = prescribed dose per fraction multiplied by the beam weighting for each field

PSF(10) = phantom scatter factor for a 10 x 10 cm field size

TMR(P/2,S) = tissue maximum ratio for the depth (half hip width) and equivalent square size S

AAF(x,y) = air area factor for collimator jaw setting (a collimator scatter factor).

PSF(S) = phantom scatter factor for equivalent field size S

ISL – inverse square law correction for the extended SAD of 400 cm

The inverse square law is:

$$\text{ISL} = \left(\frac{100}{SAD}\right)^2 = \left(\frac{100}{400}\right)^2 \quad (18)$$

Phantom Verification – TLDs

Using calculations completed on the unmodified RANDO™ phantom, a plan was developed using Radplan™ to treat the phantom with TLDs so the dose per monitor unit could be measured.

There were many reasons why TLDs were chosen as the detector for this application. These included their small size, which enabled them to fit into slots within the RANDO^{TM} phantom. TLDs have no cables attached, reusable and cost effective and have good long-term stability and negligible environmental (temperature, pressure, humidity) factors.

For the TLD measurements, the number of monitor units to be delivered was based on the effective chest width using the ratio from the homogeneous and inhomogeneous monitor units from the Radplan^{TM} planning system and rather than using the hip width for calculating the monitor units and then adding bolus as would be done for treatment, as the aim was to assess the effective chest width calculation.

The TLDs used were Harshaw TLD-100 chips, which are lithium fluoride chips doped with impurities of magnesium and titanium. The chips have a physical size of 3.2 x 3.2 x 0.89 mm and a density of 2.64 g/cm^3 and a Z_{eff} of 8.2. The TLDs are always handled with vacuum tweezers.

Prior to use, the TLD system was calibrated according to the Westmead Hospital clinical protocol. A reader calibration factor (RCF) was generated using a special calibration set of TLDs. The RCF factor is the ratio of response of the instrument in nanocoloumbs to the actual radiation to which the calibration dosimeters were exposed, i.e. converting the readings from nC to cGy.

The set of TLDs used was a set of clinical TBI TLDs, calibrated for 2 Gy exposures. Each TLD set in the chip was given an individual element correction coefficient (ECC). The ECC for each dosimeter corrects its response to produce a response equal to the average of all the dosimeters, as not all chips can be manufactured with the same TL efficiency.

The TLD chips were calibrated in a Perspex^{TM} phantom with holes drilled in it for TLDs and Farmer style ion chamber placement. Ion chamber readings are corrected for temperature and pressure. Conditions for calibrations should be as close as possible to the conditions for TLD measurement, including using beams with the same beam quality as for measurement and approximately 2 Gy being delivered to both treatment and calibration chips to reduce supralinearity effects.

Before calibration and exposure measurements, TLDs are pre-annealed for one hour at 400°C and then for two hours at 100°C. This also removes residual TL signals and establishes TLD sensitivity.

The TLDs are placed into slots within the RANDO™ phantom especially designed for TLD chips. Chips were placed into three slots on midplane about the calculation point used in the planning systems. Diagram 3.3 shows red crosses where the TLDs were positioned. It should be noted that there is some uncertainty introduced as the calculation point was in the middle of the slice whereas TLDs are to be positioned towards the edge of the slice.

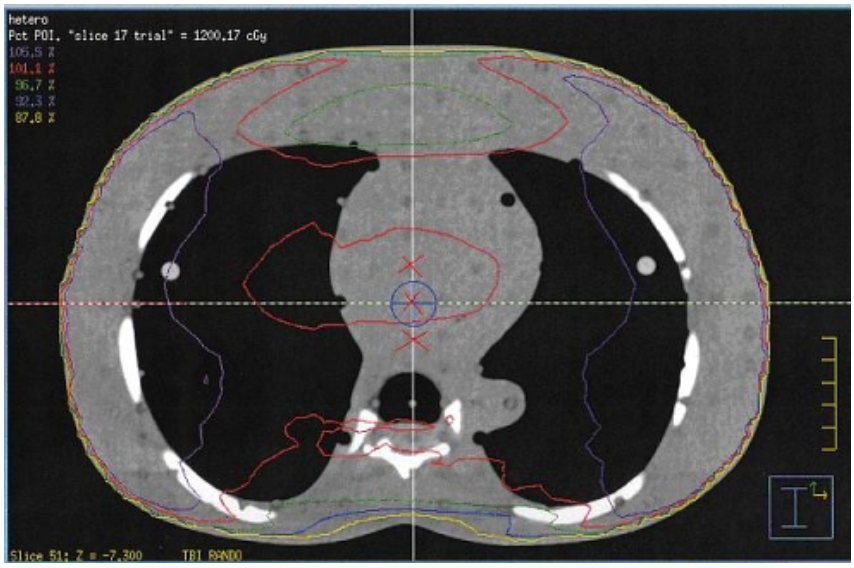

Diagram 3.3 – Placement of the TLDs at the red crosses.

The phantom was positioned on a special TBI treatment couch at an extended FAD of 4 metres as planned. The phantom was treated according to the plan, rotating the phantom after each beam. (The bunker is wider on one side of the gantry than the other, so rather then rotating the gantry to deliver the bilateral beams, the patient bed is rotated). The phantom was aligned using a special TBI laser that points down a line that is 4 metres from the source. This laser line was aligned to the midline of the phantom. This process was repeated three times for three sets of TLDs and the results averaged.

Some of the set of TLDs were reserved and are now used for scaling purposes for supralinearity correction. The scaling dose is based on an estimate of what the dose to the TLDs in the phantom was. The scaling is done in the calibration phantom, together with an ion chamber to measure absolute dose. The ion chamber reading was corrected for air density and other factors such as polarity.

After irradiation, fading occurs in TLDs, particularly in peaks not used for dosimetry. In order to hasten the fading process, TLDs are post annealed for 10 minutes at 100°C prior to being read.

The automatic Harshaw 5500 reader was used. The TLDs are read with an acquisition set up of a temperature ramp of 15°C/s to a maximum of 300°C with an acquisition time of 33 1/3 seconds.

The results from the reader are transferred as an ASCII file to a Microsoft Excel worksheet with a macro developed using Visual Basic for Applications to use the reading from the scaling TLDs and a supralinearity corrections formula (fitted to measured supralinearity curve) to correct the measured TLDs.

Phantom Verification – Film

Radiographic film was used as a two dimensional dosimeter to verify the dose distributions produced by the treatment planning systems and the differences from changing to the extended SAD used for treatment. Radiochromic film could also have been used, but radiographic film was more cost effective and available in larger sheets.

A sheet of ready-packed Kodak EDR2 film (Eastman Kodak Company, Rochester, New York) from the same batch as the films used for phantom verification was used for calibration. It was exposed to varying amounts of radiation using a 6 MV beam from a Varian 6Ex Clinac from 0.25 Gy to 4 Gy, as calculated using measured treatment planning data. 5 cm of solid water was used for backscatter and 1.5 cm of solid water was placed on top of the film. Each segment of radiation had a field size of 5 x 5 cm. The film was positioned at an SAD of 100 cm.

One envelope of ready-packed Kodak EDR2 film was positioned between slices of the anthropomorphic phantom close to the calculation point used by the treatment planning systems. The phantom slices were clamped together and were positioned at TBI treatment position (TBI extended SAD of 400 cm) and 1966 monitor units were delivered bilaterally, as per calculations based on heterogeneity correction for the RANDO^{TM} phantom produced by Pinnacle^{TM}, based a prescription of 2 Gy per fraction. The film was removed and another film positioned and the phantom repositioned so that the SAD was 100 cm. 123 monitor units were delivered bilaterally.

Pin pricks were made in one corner of each film to mark the orientation of the film and to allow for air pockets to be squeezed out of the pre packaged film envelopes to prevent hot spots developing.

The films were left overnight to stabilise its optical density response. The film envelopes were opened in the darkroom and each film was processed in an AGFA classic E.O.S. automatic film processor, dedicated to use for radiotherapy films. All the films were processed sequentially in the same batch to reduce processor variation.

Following being processed the films were digitised using a VXR-16 Dosimetry Pro 16 bit CCD film scanner (VIDAR Systems Corporation, Herndon Virginia) and the images were saved in TIFF image format.

These tiff image files were then loaded into the DoseLab 3.05 software (Childress, 2003) for analysis. The software calculates the dose at a point as being proportional to the optical density of the film.

The calibration film was used to convert optical density to dose. The films from the 100 cm and 400 cm SAD phantom verification measurements were then converted to dose and isodoses were calculated for comparison with the isodose distributions produced by the treatment planning systems.

Chapter Four – Results

CT to density calibration

Diagram 4.1 shows the calibration of Hounsfield unit (HU) to density used by Pinnacle™ and Radplan™.

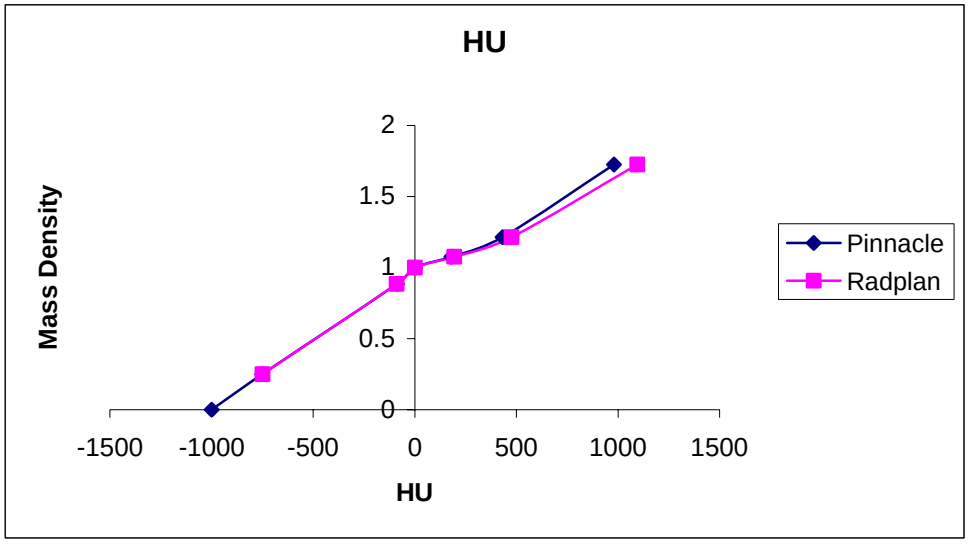

Diagram 4.1 – the Hounsfield calibration for density used by the planning systems. The Pinnacle™ system uses CT numbers so these have been converted to Hounsfield number for display.

Ratio Differences: Radplan™ and Pinnacle™

Table 4.1 shows the effective chest widths calculated using the ratio between heterogeneous and homogenous monitor units from Pinnacle™ and Radplan™ and the difference between the two models. The systematic difference arises because Pinnacle™ includes the effects of changes to scatter due to the heterogeneity. If the effective chest width is larger than the hip width, bolus is added around the hips so the effective chest width and the hip width are the same.

	Pinnacle™ effective chest width (cm)	**Radplan™ effective chest width (cm)**	**Difference**
Wide Short	20.8	20.1	3.4%
Narrow Tall	22.8	21.9	3.9%
Largest Lung	20.7	20.1	2.9%
Smallest Lung	22.7	21.9	3.5%
RANDO™	22.6	21.9	3.1%

Table 4.1 – The effective chest widths calculated using the ratios between heterogeneity and homogeneity calculations from Pinnacle™ and Radplan™ for different phantoms.

Table 4.2 shows the dose per monitor unit calculated using the effective chest width based on the ratio of homogeneous and inhomogeneous monitor units calculations produced by the treatment planning system together with the average dose per monitor unit as measured by TLDs. The standard deviation for the TLD measurements was ±4%, so both the Pinnacle™ and Radplan™ dose delivered per monitor unit agree within one standard deviation with the measured dose per monitor unit.

Calculation/measurement technique	Dose (Gy) per monitor unit at 400 cm SAD
Radplan™	0.105
Pinnacle™	0.102
TLD	0.106

Table 4.2 – Dose (Gy) per monitor unit at the extended TBI SAD of 400 cm as calculated using the ratios from Radplan™ and Pinnacle™ and measured using TLDs.

Film Dose Response

Diagram 4.2 shows the exposed film used to determine the dose response curve and diagram 4.3 shows the dose response curve obtained from the film and used for film to dose calibration.

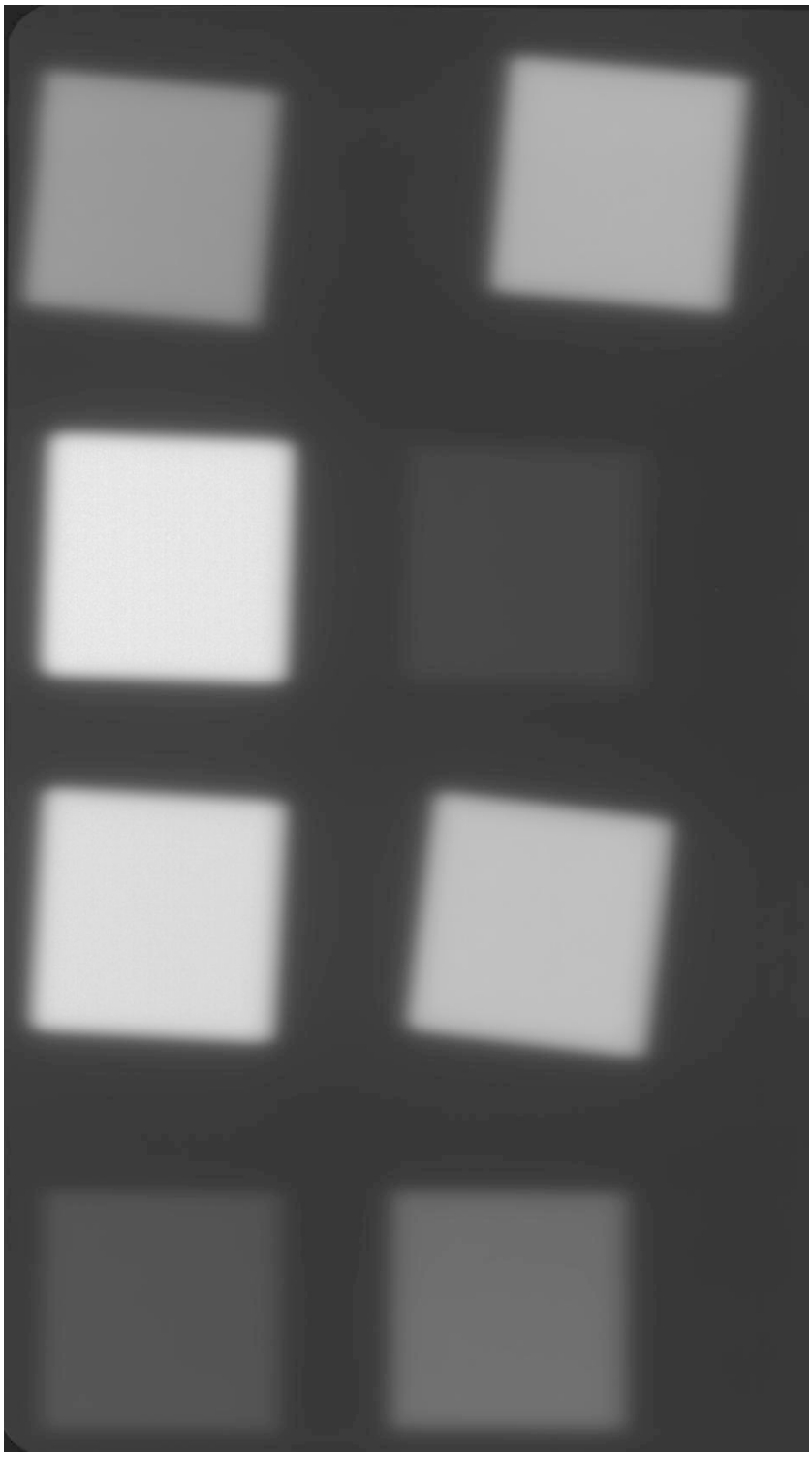

Diagram 4.2 – the calibration film used to convert optical density to dose.

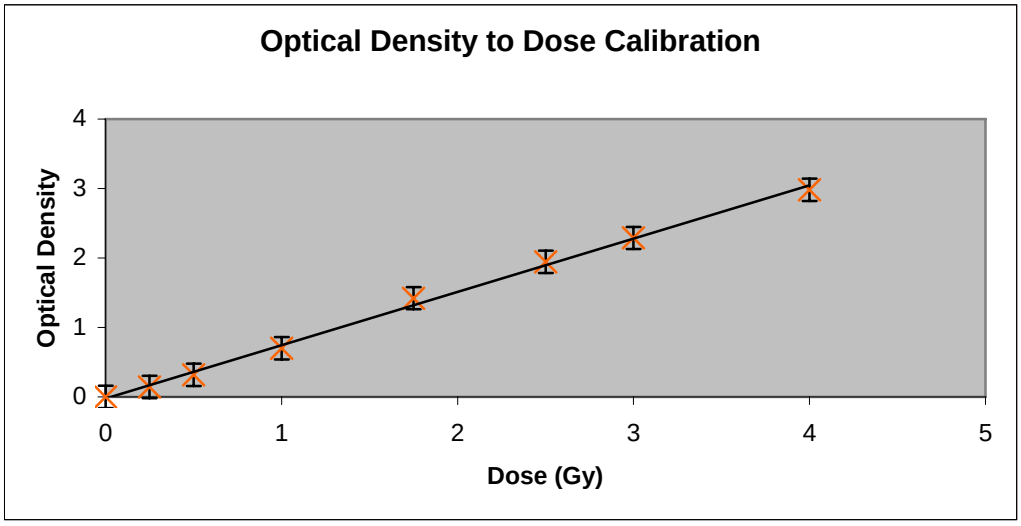

Diagram 4.3 – the calibration curve used to convert optical density to dose.

Isodose Distributions

All diagrams are normalised so that 100% of the prescribed dose is at the calculation point on central axis midline.

Diagram 4.4 shows the isodose distribution produced by Pinnacle™ for the RANDO™ phantom in the transverse plane containing the calculation point, marked by the orange cross on the isodose map. Diagram 4.5 shows the same thing for Radplan™. Diagram 4.6 shows the measured isodose distribution from the Kodak EDR2 film at an SAD of 100 cm in RANDO™, showing at least a reasonable qualitative agreement with diagrams 4.4 and 4.5. It can be seen that the measured dose as in diagram 4.6 receives a slightly higher dose in the centre of the chest than either system calculated and shows better agreement with the distribution calculated by Pinnacle™.

Diagram 4.7 shows the measured isodose distribution from Kodak EDR2 film at an SAD of 400 cm in RANDO™ and diagram 4.8 shows the calculated isodose distribution at 400 cm SAD from Pinnacle™.

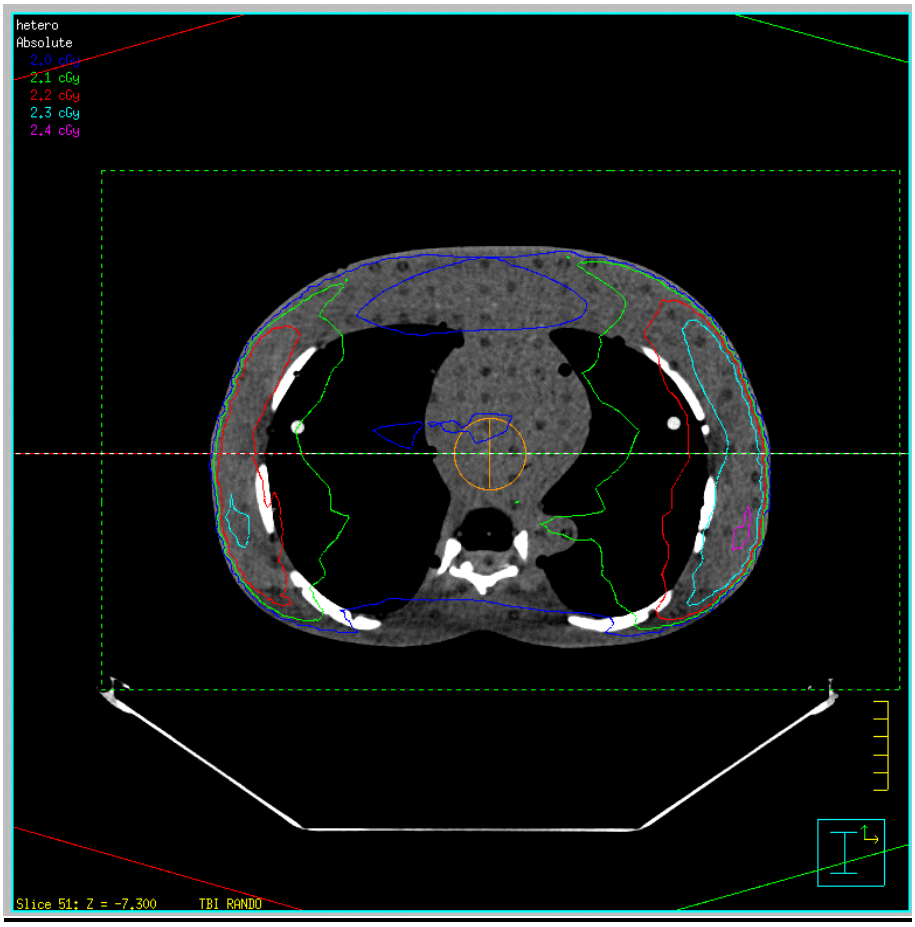

Diagram 4.4 – isodose distribution in the transverse plane at 100 cm SAD calculated by Pinnacle^{TM}.

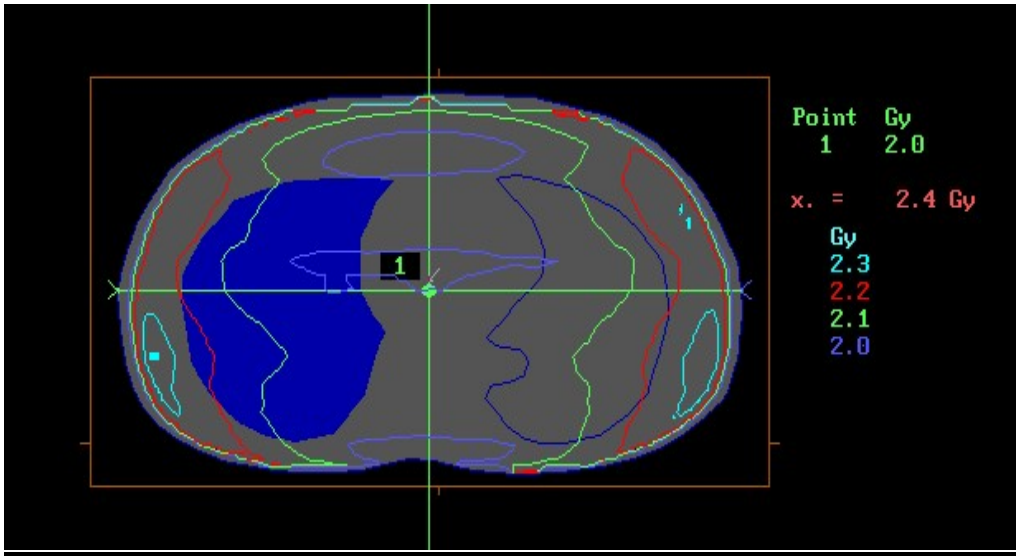

Diagram 4.5 – isodose distribution in the transverse plane at 100 cm SAD calculated by Radplan^{TM}

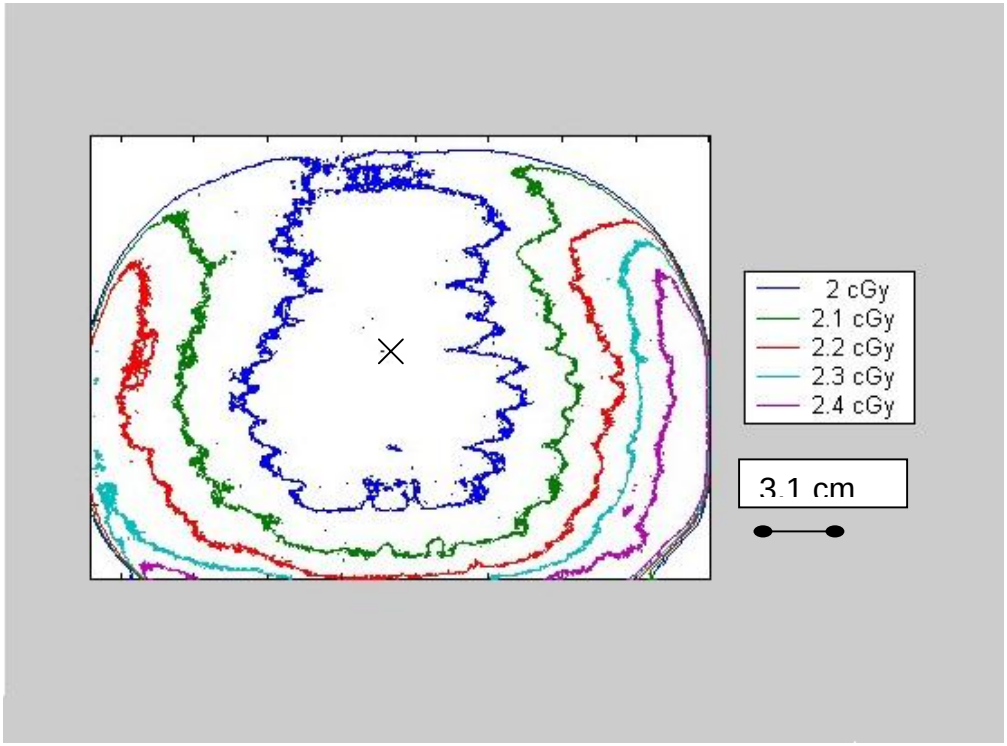

Diagram 4.6 – measured isodose distribution from film at and SAD of 100 cm in RANDO™.

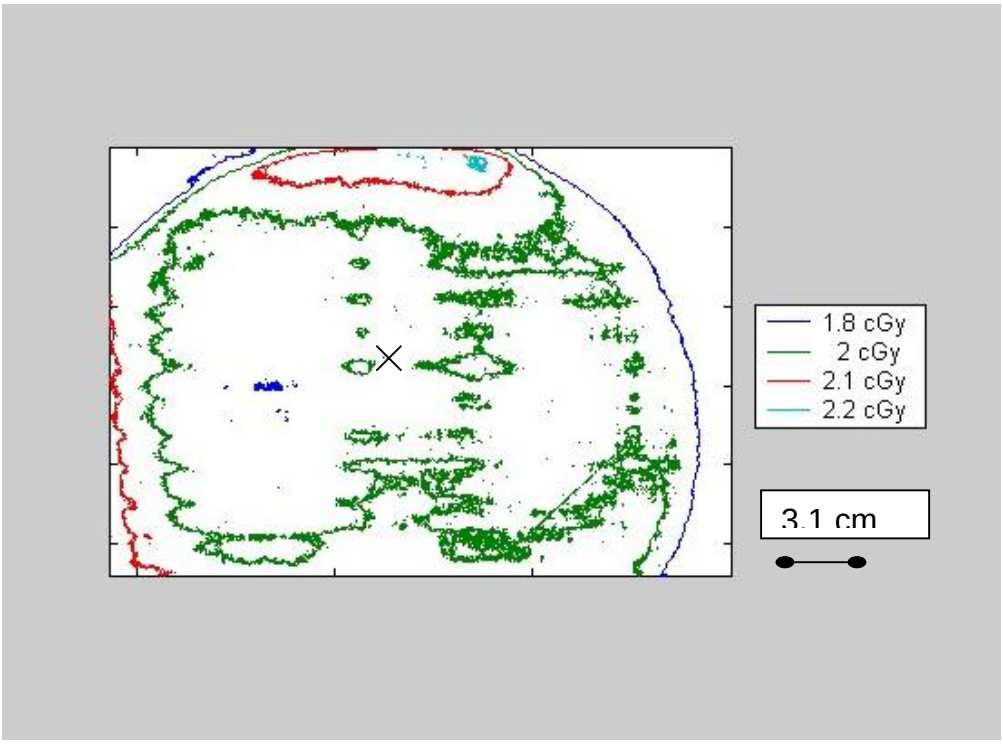

Diagram 4.7 – measured isodose distribution from film at extended SAD of 400 cm in RANDO™.

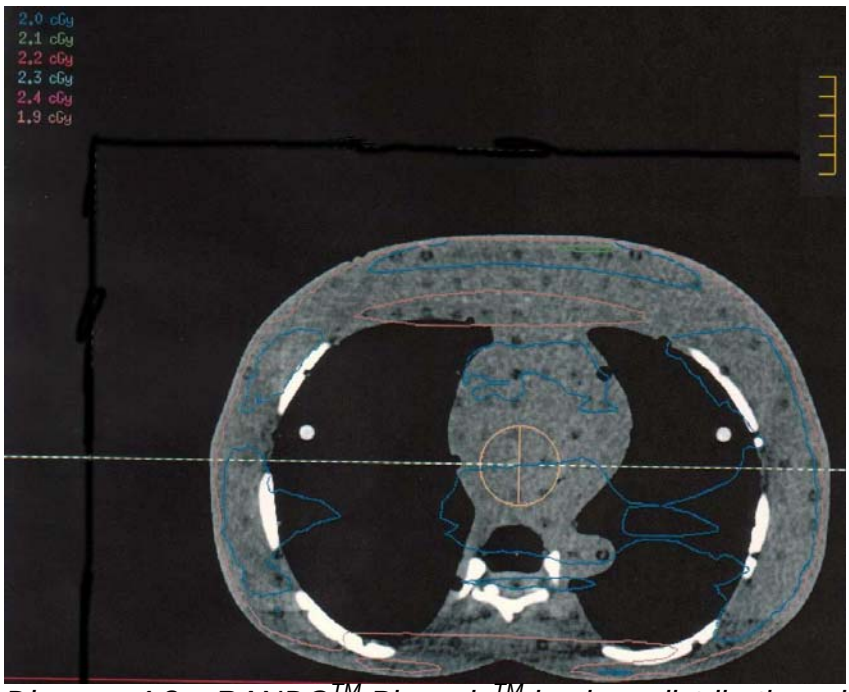

Diagram 4.8 – RANDO™ Pinnacle™ isodose distribution with heterogeneity correction at 400 cm SAD.

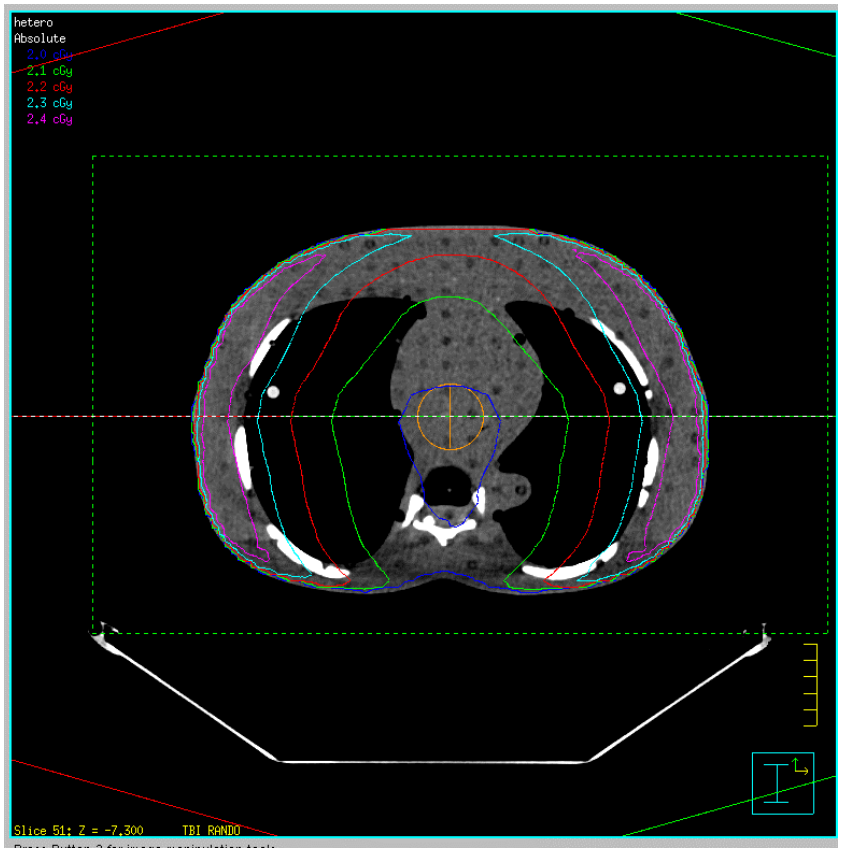

Diagram 4.9 – RANDO™ Pinnacle™ isodose distribution without heterogeneity correction at 100 cm SAD.

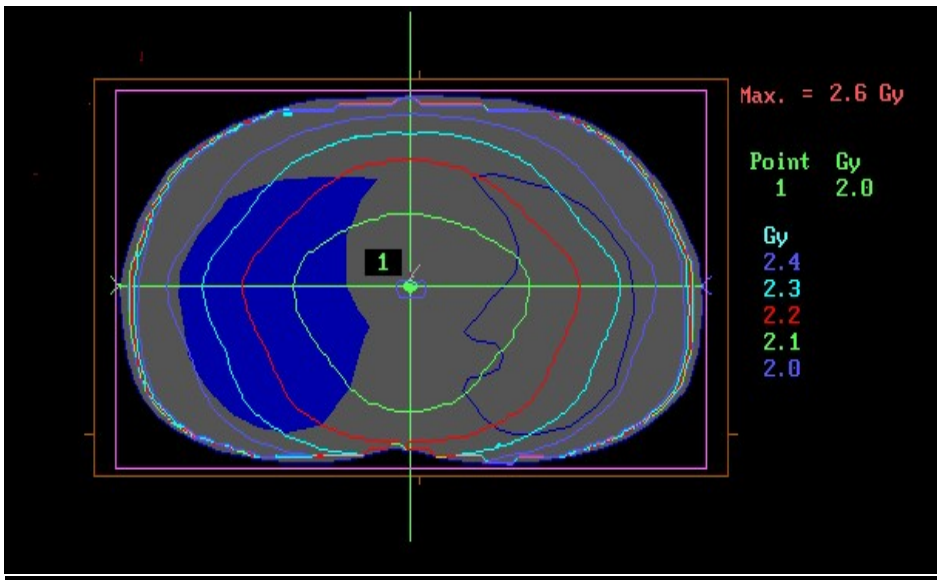

Diagram 4.10 – RANDO^{TM} RadPlan^{TM} isodose distribution without heterogeneity correction at 100 cm SAD.

Chapter five – Discussion

TBI involves complex dosimetry but the dosimetry due to the large SAD, dose uniformity and flatness over the large field, bolus requirements, extra scatter from the bunker walls and floor and large field overshoot. There is also a lack of specialised treatment planning systems for TBI planning at extended SAD.

TBI involves complex dosimetry due to the large SAD. This changes the angular distribution and electron contamination of the beam, changing the dose uniformity and flatness over the large field. TBI dosimetry is also complex due to bolus requirements, extra scatter from the bunker walls and floor and large field overshoot. There is also a lack of specialised treatment planning systems for TBI planning at extended SAD.

In this project the effective chest width for treatment monitor unit calculations and bolus requirements was calculated. This value varies between the 2D Bentley – Milan algorithm with modified Batho heterogeneity corrections and the 3D convolution method by less than 4%. The width of the lungs caused the greatest variation. Changing the height and depth of the lungs produced less than 1% variation.

Having determined the difference between Radplan^{TM} and Pinnacle^{TM} does not change significantly due to lung size, the phantom verification work was completed using RANDO^{TM}, as TLD slots were available to position the TLDs. One disadvantage with the RANDO^{TM} phantom is it doesn't have arms, which would affect the dose distributions delivered in a real patient, as the arms would provide additional shielding to the lungs. Hence TLDs were placed in RANDO^{TM} and the measurements showed that the dose per monitor unit using an effective chest width for monitor unit calculations using the ratio between heterogeneity and homogeneity calculations from Radplan^{TM} and Pinnacle^{TM} varied less than 4%. According to the AAPM TG53 report, the recommended accuracy required in calculations from a treatment planning system for a 3D calculation with heterogeneities present should be within 5%. This shows that either method of calculating the effective chest width could be used for calculating the number of monitor units for TBI treatments.

Each method also provides some isodose display information, although Pinnacle^{TM} can display this information on all transverse slices as well as sagittal and coronal views.

The sagittal and coronal views show the small air gaps between phantom slices that would not be present in a patient and that Radplan^{TM} would not have included in its calculations. These gaps would not have been perfectly reproduced during each TLD verification measurement, but it is unlikely this would have much effect on the results, especially since the results were averaged over three simulated treatments.

In order to compare the two treatment planning systems the CT calibration curves had to be compared. For densities lower than water/tissue equivalent, Radplan^{TM} and Pinnacle^{TM} calibration of density to Hounsfield number was almost the same. However, some discrepancies can be seen with higher density materials which may create some small changes between the two treatment planning systems for RANDO^{TM} due to the presence of bone. However, the ratio results for RANDO^{TM} are consistent with the RANDO lung phantom. These differences are due to changes in the CT scanner between commissioning Radplan^{TM} and Pinnacle^{TM}, but were not significant enough to change the calibration curve in Radplan^{TM}.

Another difference between Radplan^{TM} and Pinnacle^{TM} is that the beam data for Radplan^{TM} and Pinnacle^{TM} was collected at different times. Also, Radplan^{TM} directly uses the measured PDD and beam profile data to calculate the dose distribution whereas Pinnacle^{TM} uses a PDD to determine the beam energy spectrum and uses this to model the dose distribution. The same beam data is used for heterogeneity and homogeneity plans, so the ratio would cancel some of the differences from different beam data measurements or models.

For verification TLDs placed in three locations for each simulated treatment so the results of each three chips for each simulation could be averaged together, as well as over three simulations. However, as the chips covered a wider area and were not all surrounded by the 100% isodose, the TLD readings may vary slightly from 100% of dose/monitor unit. Another uncertainty inherent in the TLD positioning is that the

calculation point was in the middle of the slice but the TLDs were placed in slots at the edge of the slice.

TLDs are not as accurate as ion chambers but have the advantage of being able to be placed directly into the phantom and without concern over cable and stem irradiation. An ion chamber was not used in this project for verification, as there was nowhere to position it.

TLDs are relative dosimeters so the accuracy is determined by reproducibility. In this work the reproducibility of the TLD absorbed dose measurements had a standard deviation of 4%. This error included errors due to setup for TBI treatment, such as phantom positioning and accelerator variation.

The TLDs were scaled with the scaling chips being exposed directly after the simulated TBI treatments. This should have helped the reproducibility by cancelling out TLD batch sensitivity changes, reader changes, oven changes and accelerator output. The calibrations for ECC and RCF were also completed under similar conditions to increase reproducibility.

Kodak EDR2 film was also used as a planar dosimeter for verification of the isodose distributions produced by the treatment planning systems. A dose response curve was generated to ensure the films were exposed to radiation in the linear region of the dose response curve and to be used for optical density to dose calibration. Film response to radiation is not the same across the entire film and this could result in up to a 2% variation in the response of the film. (Williams and Thwaites, 1993) The film was also slightly smaller than the RANDO^{TM} phantom as can be seen in the phantom verification films in diagrams 4.6 and 4.7.

Kodak EDR2 film has previously been shown to have variations of less than 2% compared to ion chambers except for larger field sizes and greater depth (>15 cm) where errors in the range of 3-5% were reported (Chetty, 2002). Thus, particularly around the calculation point for TBI treatments, the dose accuracy for the film may be lower. Film also has some angular dependence and when exposed parallel to the beam, as in the calibration, rather than perpendicular to the beam, some over response may be seen. (Suchowerska, 2001)

As expected, changing the height of the lungs makes no difference to the monitor units calculated by Radplan™ for the midplane as Radplan™ is a 2D system. There was also no significant difference in the ratios when changing the height of the lungs in Pinnacle™. This is because the calculation point is out the range of the main scattered radiation from the edges of the lungs. The width of the lung made a difference for the heterogeneous calculations for both the 2D and 3D system. Because no significant variation in the ratios was observed, all further work focussed only the smallest lungs and largest lungs.

When the ratios are used to manually calculate the doses required to treat a patient with the RANDO™ lung phantom dimensions, because the effective chest width always remains smaller than the width of the hip, the monitor units for treatment remain the same. However, the plate separation would be different and hence different amounts of bolus material would be added to build up the chest to the plate separation width. This means that for cases where the effective chest width is smaller than the width of the hips for both methods of calculating the ratio for the effective chest width (Radplan™ and Pinnacle™), the only part of the body that receives a different dose would be the chest, due to the changes in bolus material added.

Isodose distributions from different planning methods and measurements can be quantitatively compared. Various methods for quantitative analysis of isodose distributions include dose differences or distance to agreement analysis, which combines both dose differences and distance to agreement. However, the software options available during this project did not allow quantitative analysis of isodose maps, so the isodose distribution maps were only visually compared.

The isodose distributions on transverse plane around the calculation point are similar between Radplan™ and Pinnacle™ but show some differences, especially anterior and posterior to the lungs, as the Bentley – Milan algorithm does not calculate differences in scatter from heterogeneities.

It is observed that there are differences in the isodose distributions between Radplan™ and Pinnacle™ even for homogeneous cases. This shows differences

between the two calculation methods, such as Radplan™ not calculating the change in scatter due to changes in patient contour.

When comparing the results between the smallest lungs and largest lungs in the RANDO™ lung phantom the doses are higher around the calculation pt in the largest lungs case. This effect is seen more in Pinnacle™, showing an increase in the scatter component from the extra lung volume not calculated in Radplan™. This is also why it is the midplane dose is higher in heterogeneous cases than homogeneous cases.

During treatment of patients, patient positioning changes, involuntary and voluntary patient motion (including breathing with changes to lung volume), changes to patient size and bolus distribution between fractions add to the potential errors of TBI treatment. Hence invivo dosimetry is critical during TBI treatments.

In the future it is possible that computer improvements, such as treatment planning computers being able to accept larger CT imaging data sets and having increased computation speeds, will aid 3D planning for TBI. The difference in measured isodose distributions between 100 and 400 cm SAD also suggests that using beam data from an extended SAD would be a future improvement so isodoses and DVHs can be more accurately used for dose evaluation if required during TBI.

Chapter Six – Conclusion

This project compared two planning methods for calculating the heterogeneity correction required for determining the effective chest width for planning TBI, taking into account possible effects of different lung sizes. The two planning methods were the 2D Bentley – Milan algorithm with modified Batho heterogeneity corrections and 3D convolution planning methods. Measurements were made in an anthropomorphic phantom with films and TLDs to verify the results.

An anthropomorphic phantom was modified with different lung size inserts and four different lung sizes were calculated on both treatment planning systems. The process was repeated using the unmodified anthropomorphic phantom, which had slots for TLD measurements for verification measurements.

For an isocentric treatment, the treatment planning system for each lung size calculated the monitor units required to deliver the prescribed dose to the midline for both with and without heterogeneity corrections.

The ratio between the number of monitor units required with and without heterogeneity corrections was used to calculate the effective chest width of the patient. This was compared to the measured hip width and the larger value was used to calculate the monitor units required to deliver the prescribed dose to the midline at TBI treatment SAD. The effective chest width varied less than 4%.

The effect of different lung sizes was only seen where the width of the lungs changed. Changes to the height or depth of the lungs had no significant effect on the calculations of the effective chest width, as was to be expected as changing the height and depth of the lungs only changes the scatter component.

The isodose distributions in the transverse plane were also measured with Kodak EDR2 film and showed reasonable agreement between the calculated and measured isodoses at isocentre. The isodose distribution changed significantly at the extended TBI treatment SAD of 400 cm. However, the changes showed a more uniform dose distribution at the extended SAD, as expected.

The dose per monitor unit at treatment SSD was then calculated for the TBI treatment SSD without any bolus or tissue compensation based on the effective chest width from both planning systems and this was compared to a dose per monitor unit value measured in RANDO^{TM} using TLDs.

Whilst the heterogeneity corrections were different between the planning systems, The difference was smaller than one standard deviation of measurements from the TLDs, so no significant difference could be detected between each planning method and the TLD measurements, which had an accuracy of 4%. This is within the 5% accuracy required. The isodose distributions produced by both treatment planning systems showed reasonable agreement with the isodose measurements taken at isocentre. This shows that either method of planning TBI would be suitable for clinical purposes.

References

1. Harden SV, Routsis DS, Geater AR et al. Total body irradiation using a modified standing technique: a single institution 7 year experience. BJR 74: 1041 – 1047, 2001

2. Cosset JM, Socie G, Dubray B et al. Single dose versus fractionated total body irradiation before bone marrow transplantation: radiobiological and clinical considerations. Int J Radiat Oncol Biol Phys. Sep;30(2):477-92, 1994

3. Shank B, Chu FC, Dinsmore R et al. Hyperfractionated total body irradiation for bone marrow transplantation. Results in 70 leukemia patients with allogenic transplants. Int J Radiat Oncol Biol Phys. Nov;9(11):1607-11, 1983

4. International commission on Radiation Units and Measurements. Prescribing, recording and reporting photon beam therapy. Report 50. Bethesda, MD: ICRU, 1993.

5. Sanchez-Doblano F. Quast U, Arrans R et al. Reporting total body irradiation prior to bone marrow transplantation. ISBN: 84-605-3132-5, EBMT, Sevilla, 1995

6. Vollans SE, Perrin B, Wilkinson JM et al. Investigation of dose homogeneity in paediatric anthropomorphic phantoms for a simple total body irradiation technique. BJR Br J Radiol. Mar;73(867):317-21, 2000

7. Sanchez-Nieto B, Sanchez-Doblano F, Terron JA. A CT-aided PC based physical treatment planning of TBI: A method for dose calculation. Radiother and Oncol. 42:77-85, 1997

8. Abraham D et al. TBI treatment planning using the ADAC Pinnacle Treatment planning system. Med Dosim. 25(4):219-224, 2000

9. Smith CL, Chu WK, Goede MR et al. An analysis of the elements essential in the development of a customised TBI program. Med Dosim. 21(2):49-60, 1996

10. Sanchez-Nieto B, Sanchez-Doblano F, Arrans R et al. Backscatter correction algorithm for TBI treatment conditions. Med Dosim. 18:107-111, 1993

11. Curran WJ, Galvin JM, D'Angio GJ. A simple dose calculation method for total body photon irradiation. IJROBP 17:219-24, 1989

12. AAPM Report 17. The physical aspects of total and half body photon irradiation. Editors: Van dyk J, Galvin JM, Glasgow GP, Podgorsak EB. Task Group 20 of the Radiation Therapy Committee of the American Association of Physicists in Medicine, 1986.

13. Rider WD, Van Dyk J. Total and partial body irradiation. In: Radiation therapy Treatment Planning.. Editors: Bleehan NM, Glatstein E, Haybittle JL. Marcel Dekker, New York, 559-594, 1983.

14. Van Dyk J. Dosimetry for total body irradiation. Radiother Oncol. 9:107-118, 1987.

15. Mayneord WV, Lamerton LF. A survey of depth dose data. BJR 14:255, 1944

16. Doughty D, Lambert GD, Hirst A et al. Improved total-body irradiation dosimetry. BJR 60;269-78, 1987.

17. Fiorino C, Mangili P, Cattaneo GM et al. Polarity effects of ionisation chambers used in TBI dosimetry due to cable irradiation.

18. De Sapio E et al. Optimization of a dosimetric procedure in total body irradiation. Radiol Med Torino Jun;79(6):624-7, 1990.

19. Quast U. Physical problems of total body irradiation. Strahlenther Onkol. 1986 Apr;162(4):233-6.

20. Khan FM. The Physics of Radiation Therapy. 2nd Ed. Baltimore: Williams and Wilkins; 2003.

21. Obcemea CH, Rice RK, Mijnheer BJ et al. Three-dimensional dose distribution of total body irradiation by a dual source total body irradiator. IJROBP 24:789-793, 1992

22. Amor Duch M, Ginjaume M, Chakkor H et al. Thermoluminescence dosimetry applied to in vivo dose measurements for total body irradiation techniques. Radiother Oncol. 47:319- 324, 1998

23. Khan FM, Williamson JF, Sewchand W et al. Basic data for dosage calculation and compensation. IJROBP 6:745-751 (1980)

24. Svahn-Tapper G, Nilsson P, Jönsson C et al. Calculation and measurements of absorbed dose in total body irradiation. Acta Oncol 29 (1990)

25. ICRU 21. Radiation Dosimetry: Electrons with initial energies between 1 and 50MeV. International Commission on Radiation units and Measurements. Report No 21, Washington DC, USA 1972.

26. Syh HW, Chu WK, Kumar P et al. Estimation of the mean effective organ doses for total body irradiation from RANDO phantom measurements. Med Dosim. 17:103-106, 1992.

27. Kirby TH, Hanson WF, Cates DA. Verification of total body photon irradiation dosimetry techniques. Med Phys. 15(3): 364-369, 1988

28. Podgorsak EB, Pla C, Evans, DC et al. The influence of phantom size on output, peak scatter factor, and percentage depth dose in large-field photon irradiation. Med Phys 12(5): 639-645, 1985

29. Yuille PG, Wielinga W, Crestani EA. Fractionated total body irradiation in bone marrow transplantation – an emphasis on lung dosimetry. Australas Radiol 27: 186-194, 1983.

30. Metcalfe P, Kron T, Hoban P. The physics of radiotherapy x-rays from linear accelerators. Medical Physics Publishing. 1997

31. Quast U. Dosimetry of Total Body Irradiation – A review. Dosimetry in Radiotherapy Vol 2, Proceedings of a symposium Vienna, 31 August – 4 September 1987 IAEA

32. International commission on Radiation Units and Measurements. Dose Specification for Reporting External Beam Therapy with Photons and Electrons. Report 29. ICRU, 1978.

33. El-Khatib E, Battista JJ. Accuracy of lung dose calculations for large-field irradiation with 6-MV x rays. Med Phys 13(1): 111-116, 1986

34. Lulu BA, Bjarngard BE. Batho's correction factor combined with scatter summation. Med Phys 9(3): 372-7, 1982

35. Butson MJ, Elferink R, Cheung T et al. Verification of lung dose in an anthropomorphic phantom calculated by the collapsed cone convolution method. Phys Med Biol 45 (11): N143 –149, 2000

36. Batho HF. Lung corrections in Cobalt 60 beam therapy. J. Can. Assoc. Radiol. 15: 79 – 83, 1964

37. Sontag MR, Cunningham JR. Corrections to absorbed dose calculations for tissue inhomogeneities. Med Phys 18(4):719 – 723, 1991

38. Webb S, Fox RA. The direct use of CT data for inhomogeneity corrections in radiotherapy planning. Br. J. Radiol. Suppl 15, 1979

39. International commission on Radiation Units and Measurements. Tissue substitutes in radiation dosimetry and measurement. Report 44. ICRU, 1989

40. The Merck Manual of Diagnosis and Therapy. 17th Edition. Edited by Beers MH and Berkow R. 1999-2005, Merck & Co.

41. Bomford CK and Kunkler IH. Walter and Miller's Textbook of Radiotherapy. 6th Ed. Elsevier Science Limited. 2003

42. Williams JR and Thwaites DI. Radiotherapy physics in practice. Oxford University Press. 1993

43. IAEA TRS 398. Absorbed dose determination in external beam radiotherapy: an international code of practice for dosimetry based on standards of absorbed dose to water. International Atomic Energy Agency. 2000

44. AAPM TG53. Quality assurance for clinical radiotherapy treatment planning. Editors: Fraass B, Doppke K et al. Task Group 53 of the Radiation Therapy Committee of the American Association of Physicists in Medicine, 1998.

45. International commission on Radiation Units and Measurements. Determination of absorbed dose in a patient irradiated with beams of X or gamma rays in radiotherapy procedures. Report 24. ICRU, 1976

46. Chilress NL, Salehpour M, Dong L et al. Dosimetric accuracy of Kodak EDR2 film for IMRT verifications. Med Phys 32(2): 539-48, 2005

47. Bucciolini M, Buonamici FB, Casati M. Verification of IMRT fields by ilm dosimetry. Med Phys 31:161-168, 2004

48. Childress NL, Rosen II. Effect of processing time delay on the dose response of Kodak EDR2 film. Med Phys 31(8):2284-8, 2004

49. Dogan N, Leybovich LB, Sethi A. Comparative evaluation of Kodak EDR2 and XV2 films for verification of intensity modulated radiation therapy. Phys med Biol 47(20):3629-3641, 2002

50. Ekstrand K, Greven K, WU K. The influence of x-ray energy on lung dose uniformity in total-body irradiation. Int J Rad Biol Phys Jul 38(5):1131-6, 1997

51. Chetty IJ, Charland PM. Investigation of Kodak extended dose range (EDR) film for megavoltage photon beam dosimetry. Phys Med Biol 47(22):4121-30, 2002

52. Childress NL, Rosen I. DoseLab 3.05 – An open source dose comparison software package for medical physicists. Nov 2003

53. Thomas ED. Total body irradiation regimens for marrow grafting. Int J Rad Biol Phys 19:1285-8, 1990

54. Galvin JM, D'Angio GJ, Walsh G. Use of tissue compensators to improve the dose uniformity for total body irradiation. Int J Rad Biol Phys 6:767-771, 1980

55. Kim TH, Khan FM, Galvin JM. A report of the work party: comparison of total body irradiation techniques for bone marrow transplantation. Int J Rad Biol Phys 6:779-784, 1980

56. ICRP Publication No. 44. Protection of the patient in radiation therapy. Annals of the ICRP 15(2), 1985

57. Milan J, Bentley RE. The storage and manipulation of radiation dose data in a small digital computer. Br J Radiol. 47(554):115-21, 1974

58. Storchi P, Woudstra E. Calculation of the absorbed dose distribution due to irregularly shaped photon beams using pencil beam kernels derived from basic beam data. Phys Med Biol, 41(4):637-56, 1996

59. Johns HE, Cunningham JR. The Physics of Radiology. 4th Ed. Charles C Thomas Publisher. 1983

60. IEC 61217 Radiotherapy Equipnment – Coordinates, Movements and Scales (Consolidated edition), 2002.

61. Suchowerska N, Hoban P, Butson M et al. Directional dependence in film dosimetry: radiographic and radiochromic film. Phys Med Biol, 46 (5):1391 – 1397, 2001